NOAA Technical Report ERL 369-WPL 46

Refractive Index Variance and its Height Distribution in Different Air Masses

Earl E. Gossard

June 1976

U.S. DEPARTMENT OF COMMERCE
National Oceanic and Atmospheric Administration
Environmental Research Laboratories

Geophysicist Dr. Earl Everett Gossard is Chief of the Meteorological Radar Program, Wave Propagation Laboratory, NOAA/ERL, Boulder, Colorado. Dr. Gossard was for many years head of the Radio Physics Division at the Naval Electronics Laboratory Center, San Diego, California. A native of Eureka, California, Dr. Gossard obtained an AB degree from the University of California at Los Angeles, and MS and PhD degrees from the University of California at San Diego (La Jolla)

He is a member of Commissions II and III of the International Radio Scientific Union (URSI). He is also a member of the URSI National Committee and served as associate editor of Radio Science from 1966-1967.

Dr. Gossard has published more than 50 papers in technical journals and is co-author (with W. H Hooke) of a book entitled Waves in the Atmosphere, published by Elsevier, Amsterdam, in 1975.

He received the annual award for outstanding scientific achievement at the Naval Electronics Laboratory Center in 1971 and an award given by NOAA/ERL for outstanding authorship in 1976.

NOAA Technical Report ERL 369-WPL 46

Refractive Index Variance and its Height Distribution in Different Air Masses.

Earl E. Gossard

Wave Propagation Laboratory
Boulder, Colorado

June 1976

U.S. DEPARTMENT OF COMMERCE
Elliot Richardson, Secretary

National Oceanic and Atmospheric Administration
Robert M. White, Administrator

Environmental Research Laboratories
Wilmot Hess, Director

CONTENTS

REFRACTIVE INDEX VARIANCE AND ITS HEIGHT DISTRIBUTION IN DIFFERENT AIR MASSES

Earl E. Gossard

With the advent of radars capable of detecting backscatter from turbulent inhomogeneities in the clear air, there is renewed interest in the refractive character of the atmosphere. The radio refractive index structure function and its spatial and temporal distribution are of particular importance.

The general refractive properties of air masses and their associated frontal discontinuities are discussed in this report, and the refractive index distribution with height is calculated. Based on certain assumptions, the distribution of refractive index structure constants is then deduced and the results are compared with the limited observational data available.

Introduction

The coverage of microwave radar and communications systems depends critically on the refractive structure of the atmosphere, and its refractive properties have been investigated for many years (see Kerr, 1951; Bean and Dutton, 1966). It has also been long recognized that turbulent fluctuations in atmospheric refractive index can produce a kind of Bragg scattering of energy beyond the geometrical horizon that can greatly extend the coverage of microwave communications systems (Booker and Gordon, 1950). However, such scattering strongly favors the forward direction and seems to be of little interest for monostatic radar systems, although a long lasting controversy developed about the subject of "angels" producing radar returns from the clear air. One school of thought argued that the returns were indeed from refractive index fluctuations in the clear air, while another argued that they were from birds or insects. With the advent of powerful, narrow-beam radar systems with sophisticated processing capabilities, such as the NASA radar at Wallops Island and the Lincoln Laboratory radar at Millstone Hill in the U.S.A., and the Royal Aircraft Establishment's radar at Defford, England, it became evident that returns from the clear air could, in fact, occasionally be detected (Browning, 1972; Hardy, 1972; Ottersten, 1969).

A further breakthrough occurred with the development of a frequency modulated, continuous wave radar (FM-CW) sounder capable of sensing targets very close to the radar, thus taking advantage of the inverse-range-squared strength of the received signal to study the lower atmosphere (Richter, 1969). This sounder also had a capability of viewing the atmosphere with very fine resolution, and it was immediately evident that there were commonly returns both from diffuse clear air structures (Gossard *et al.*,

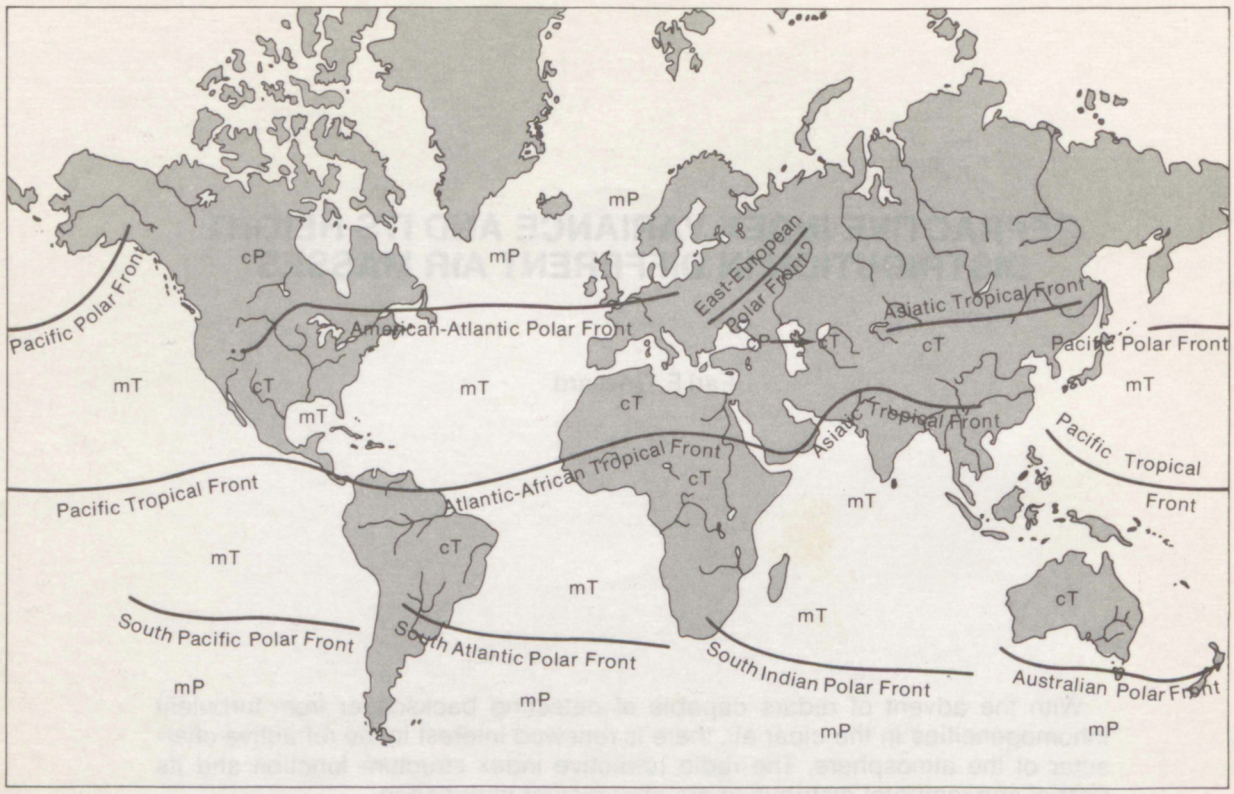

Figure 1a. Mean global air mass distribution for summer (adapted from Chromov, 1937).

1970) and from point targets such as insects and birds (Atlas *et al.*, 1970). More recently a Doppler capability of measuring the velocity of distributed, clear air targets has been demonstrated in a microwave FM-CW radar at NOAA's Wave Propagation Laboratory (Strauch *et al.*, 1976), and actual wind profiles have been measured in the clear air to a height of about 2 km (Chadwick *et al.*, 1976). The potential of microwave radars not only for sensing the refractive index turbulence structure, but also for measuring the atmospheric wind velocity distribution, creates fresh interest in the influence of meteorological conditions on the atmospheric refractive index and particularly their influence on the intensity of refractive index fluctuations and their spatial spectrum.

One approach to associating meteorology with changes in refractive index structure is through the classification of air masses and the mechanisms of their modifications. This report includes a description of one air mass classification system and a discussion of the transfer and dynamical processes by which air masses are modified. The radio refractive index is then analyzed and its dependence on the meteorological variables summarized. Special emphasis is placed on the relationship of refractive index variance to the variance of meteorological properties. Mean refractive index profiles are calculated for the various air masses. Furthermore, height profiles of the ratio of the radio refractive index structure constant to the temperature structure constant are calculated. This ratio is believed to be important because many more measurements of optical refractive index structure constant (which depends only on temperature) have been made than of radio refractive index. In fact, a tentative model of the height variation of optical refractive index structure has been proposed by Hufnagel (1974).

This report attempts to "calibrate" the radio refractive index structure constant using the Hufnagel optical model and thus to deduce absolute quantities from what would otherwise be only a relative comparison between air mass types. Finally, the deduced height distributions of refractive index structure function are compared with the very limited amount of observational data that exist—data collected by the powerful Millstone Hill L-Band radar of Lincoln Laboratory (Crane, 1970; unpublished).

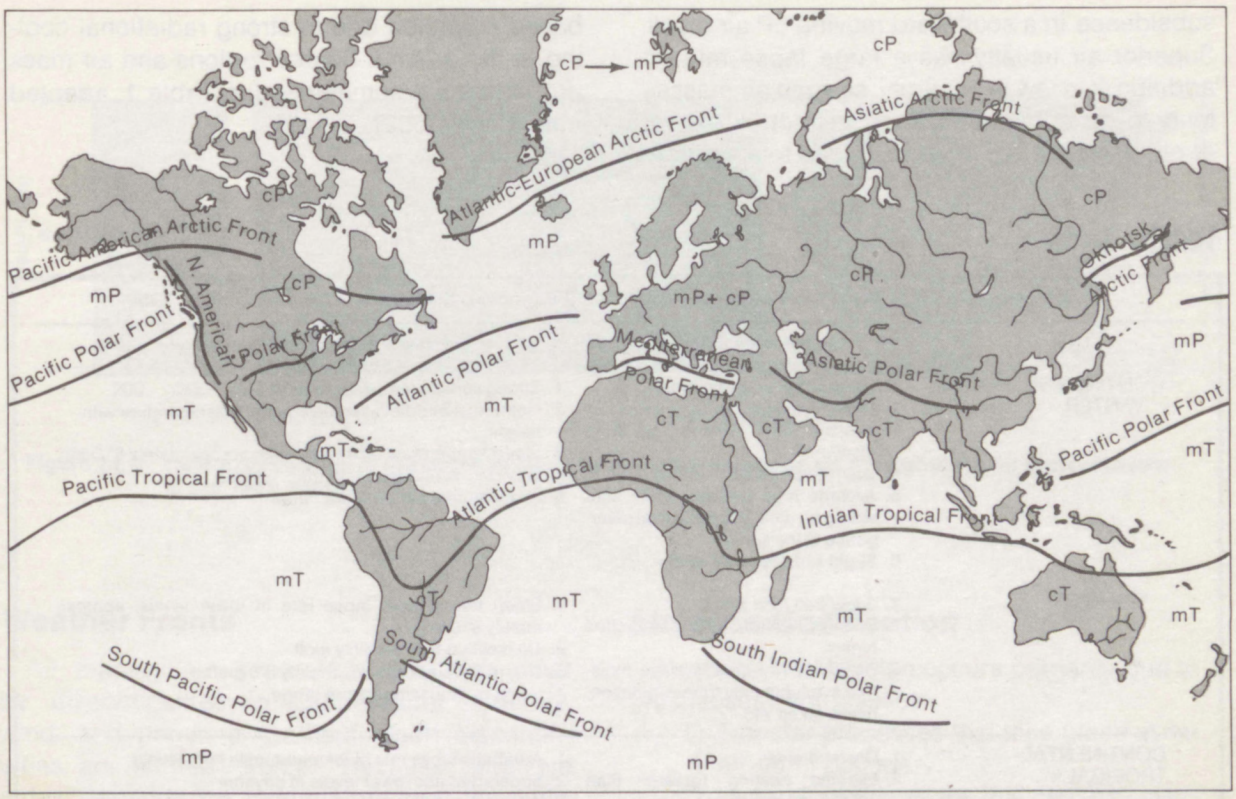

Figure 1b. Mean global air mass distribution for winter (adapted from Chromov, 1937).

Air Mass Classification

An air mass is an extensive portion of the earth's atmosphere with meteorological properties which approximate horizontal homogeneity. Thus the refractive index within an air mass is also approximately horizontally homogeneous.

One classification of air masses divides them into two basic types according to latitude in the northern hemisphere. Those originating in sources north of approximately 40° lat. are designated "arctic" (A) or "polar" (P), depending on their temperature, and those originating south of 40° lat. are called "tropical" (T). Source regions are classified as "primary" and "secondary." A primary source region is an extensive area favorable to air stagnation for appreciable periods of time. A secondary source region is one in which stagnation does not occur, but in which the air trajectories are so long that the air mass takes on characteristics associated with the underlying surface.

The two air mass types, polar and tropical, are further subdivided according to the nature of the surface in the source region. Air masses originating over snow, ice, or land surfaces are called continental, while those originating over the sea are called maritime. Continental air masses are designated by a lower case c preceding the capital P or T designations and a lower case m indicates maritime. The average location of the various air masses is shown for January and July in Fig. 1a,b (adapted from Chromov, 1937).

Further subclassifications are often used. Probably the most common indicates the temperature of the air mass relative to the surface over which it is passing. If the air mass is warmer than the surface, a lower case "w" follows the capital P or M, and if it is colder it is so designated with a lower case "k". Air masses with the k designation are thermally unstable, gusty, and turbulent with cumuliform clouds and showers. Those with the "w" designation are stable with steady winds, stratiform clouds, and drizzle.

In addition to the air masses described above, a third classification called "Superior" is often used. This describes a mass of air formed at high levels in the atmosphere. However, this air mass may, on occasion, descend to the surface of the earth. In midwestern United States this most commonly occurs during sustained

subsidence in a southward moving cP air mass. Superior air usually has a large lapse rate; in addition, it is low in humidity, so such air masses tend to be comparatively subrefractive except at night when clear skies may lead to a surface-based inversion due to strong radiational cooling at the ground. Source regions and air mass properties are summarized in Table 1, adapted from Plank (1952).

Table 1.

Meteorological Properties in Air-Mass Source Regions (Petterssen, 1940; Willett, 1944; Anderson, 1951)

Type	Source-Region Characteristics	Air-Mass Properties in Source Region
CONTINENTAL-POLAR WINTER	1. Land, snow, or ice surface 2. Excessive outgoing radiation 3. Average 80% reflection of sun's insolation 4. Low temperature; −25° to −50° C 5. Average high pressure, with subsiding air aloft and horizontal divergence at the surface 6. Slight surface evaporation	1. Strong surface temperature inversion 2. Isothermal middle layer (no change of temperature with height) 3. Steep temperature lapse rate aloft; approximately 8° C/km 4. Very dry; mixing ratio less than 1 gm/kg 5. Small diurnal temperature range
SUMMER	1. Snow-free land areas 2. Strongly-heated, long days, short nights 3. Relatively dry area, surface moisture available only from vegetation, rivers, lakes, etc.	1. Steep temperature lapse rate in lower levels; approximately 8° C/km 2. Convective-type stability aloft 3. Dry; mixing ratio approximately 5-6 gm/kg 4. Large diurnal temperature range
CONTINENTAL-TROPICAL*	1. Dry land area 2. Extreme heating (greater than 30° C during daytime) 3. Thermally created low surface pressure with high-level anti-cyclone aloft	1. Adiabatic lapse rate of temperature to high levels 2. Superadiabatic lower levels in daytime 3. Warmest possible air 4. Mixing ratio of 3-4 gm/kg; very dry at all levels 5. Large diurnal temperature range
MARITIME-POLAR WINTER	1. Ocean surface 2. Water relatively warm compared with air in western section; in central and eastern sections, air and water temperatures approach equilibrium 3. General low pressure 4. Convergence 5. Rapid moisture lapse near surface	Western Section 1. Steep to superadiabatic temperature lapse rate in the first 50-100 ft. above the sea surface 2. Convectively unstable lower levels 3. Steep lapse rate aloft 4. Rapid decrease of moisture in first 50-100 ft. 5. Little diurnal temperature variation Eastern Section 1. Convectively unstable lower strata; temperature lapse rate approximately 6-7° C/km 2. Uniform moisture distribution with height; mixing ratio averages 6-8 gm/kg 3. Cold and dry above 10,000 ft. 4. Little diurnal temperature variation
SUMMER	1. Ocean surface 2. General moderate pressure with weak gradients 3. Water temperatures which may be warmer or colder than air	1. Convectively unstable lower layers to 6,000 or 8,000 ft; lapse rate about 8° C/km 2. Uniform moderate decrease of moisture with height 3. Dry aloft, with subsidence above the level of convection 4. Slight diurnal temperature variation
MARITIME-TROPICAL SUMMER	1. Ocean surface 2. Water temperature approximately 25-28° C 3. Average high pressure 4. Weak air flow	1. Moderately steep lapse rate, approximately 7-8° C/km 2. Convectively unstable below 6,000 to 10,000 ft. 3. Very moist air; surface mixing ratios range from 18-24 gm/kg 4. Large moisture gradient to top of convective mixing layer 5. Subsiding air aloft, which tends to cap convective activity 6. Little diurnal temperature variation
WINTER	1. Ocean surface 2. Water warmer than adjacent land; water temperature average 20-23°C 3. Average high pressure 4. Weak air flow	1. Moderately steep lapse rate, 7-8° C/km 2. Convectively unstable below 8,000 to 10,000 ft. 3. Moist air; surface mixing ratios range from 13-15 gm/kg 4. Moderate uniform decrease of moisture with height 5. Subsidence above level of convection 6. Little diurnal temperature variation

*Because the characteristics and properties of both summer and winter cT air are essentially the same, only summer is covered.

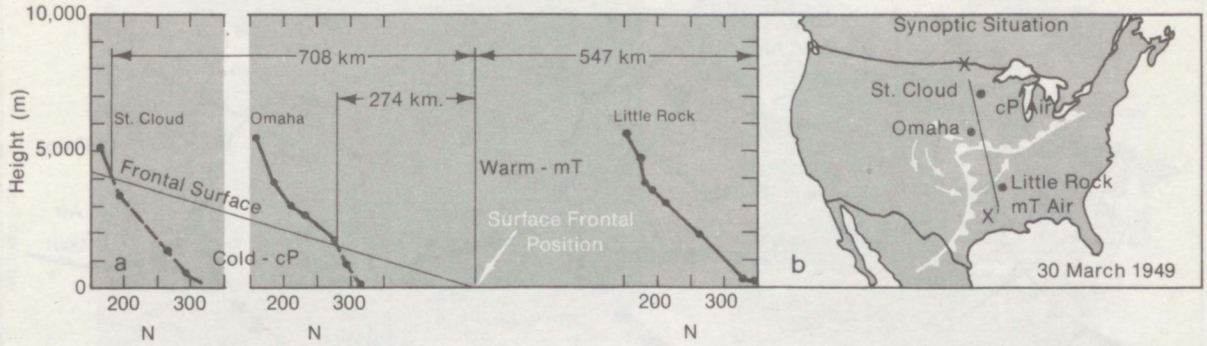

Figure 2a, b **Height distribution of refractive index N (left frame) along line xx′ through a frontal system shown in the right frame.**

Weather Fronts

Air masses are separated from each other by discontinuities in temperature, humidity, wind, and pressure gradient. Such discontinuities are termed "fronts." Because refractive index depends on temperature and humidity, it is to be expected that the fronts may sometimes have important effects on the propagation of radio and radar transmissions. An example of the way in which a front can modify the refractive index along a radio path is shown by the soundings in Fig. 2b taken along the line xx′ in Fig. 2a at the locations indicated.

Figs. 3a and 3b are schematic representations of various types of fronts. Fig. 3a shows plan views of frontal patterns at the earth's surface and Fig. 3b shows vertical sections through the fronts at the locations indicated by the line segments cc′, xx′, ww′, yy′. The figure illustrates a warm front, a cold front, and a frontal occlusion (one front riding aloft over another). Cold fronts are typically indicated by pointed bumps, warm fronts by rounded bumps and occluded fronts by hollow bumps spaced uniformly along the frontal surface.

In what follows, we will analyze the refractive structure of air masses and frontal surfaces and examine their effects on the propagation of short radio waves. ■

Air Mass Modification

Air mass modification occurs primarily due to two classes of processes:

1) Transfer processes that take place at the air-earth boundary.
2) Dynamical processes that cause convergence and divergence within the air mass.

The first class of processes includes transfer of heat, moisture, or momentum between the atmosphere and the earth's surface. Transfer processes are especially active when a dry continental or arctic air mass moves out over a relatively warm sea surface. However, significant modification of the surface layers also occurs when air moves over a relatively cooler surface. An example of the modification of the refractive structure in the lower layers as air moves southward from its source region in central Canada is shown in Fig. 4. Refractive index can also be modified by transfer processes that result from radiational heating or cooling. Temporal changes in structure then occur that are somewhat analogous to spatial changes that result from transport over a different surface. Diurnal radiational cooling of the earth-air interface is an important example of this kind of modification. In the calculation of mean refractive index structure and refractive variance for air masses, it must be remembered that an important diurnal variation in the lower layers should in fact be superimposed on the means. Temporal changes can also occur over a much longer time span due to radiational cooling when a winter air mass stagnates for a considerable length of time in an arctic

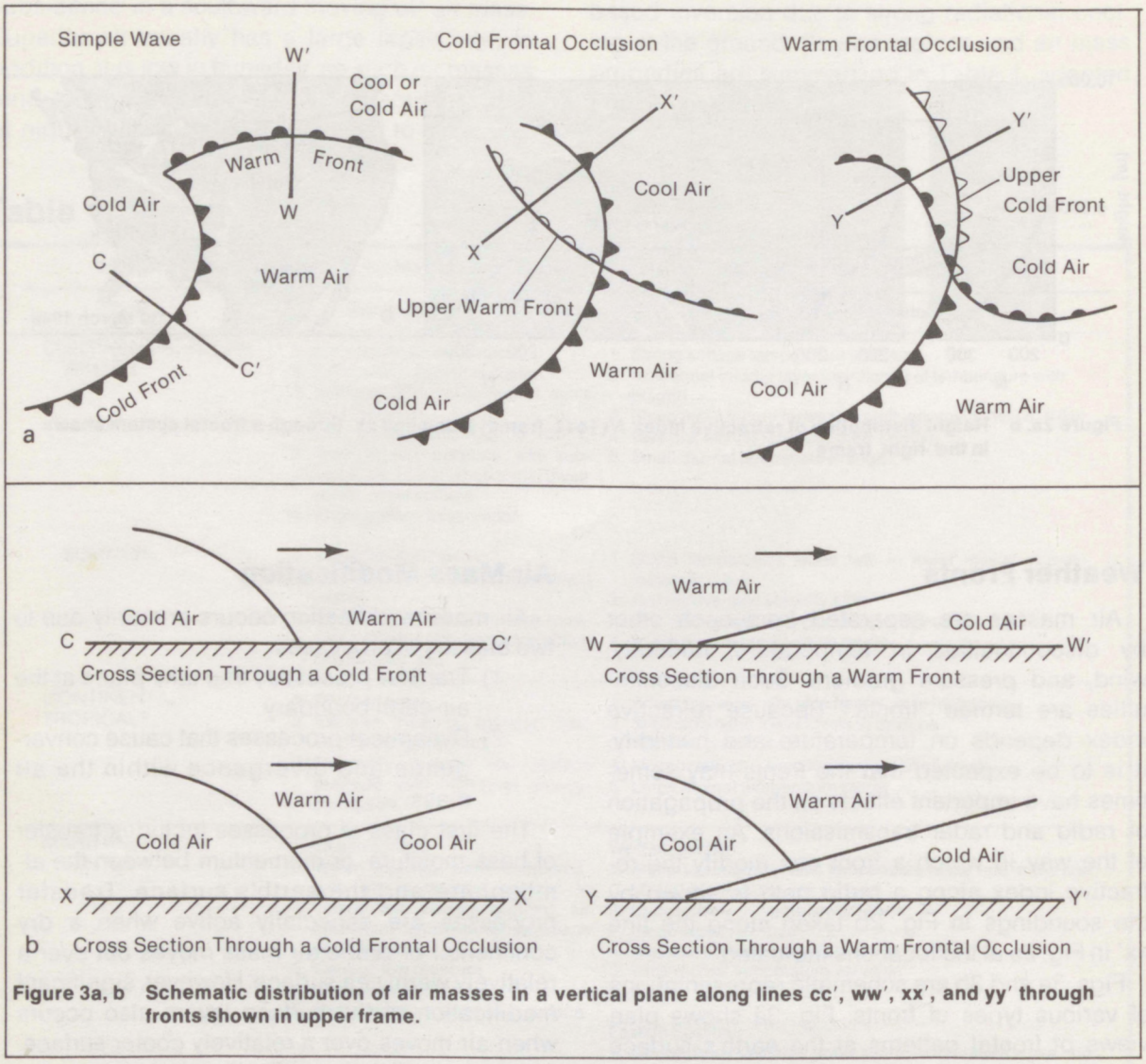

Figure 3a, b Schematic distribution of air masses in a vertical plane along lines cc′, ww′, xx′, and yy′ through fronts shown in upper frame.

source region. An example is shown in Fig. 5 which illustrates the progressive cooling of the surface layers of an air mass at Fairbanks, Alaska.

The second class of processes results in stretching or subsidence within the air mass. If stretching due to convergence takes place, the air mass will tend towards thermal instability and turbulent mixing, its temperature lapse will approach the adiabatic, and the potential refractive index* gradient will tend toward zero. The refractive index variance will be small compared with that of stratified air masses for a given intensity of mechanical mixing. Such convergence is typically associated with a northward-moving cyclonic trajectory.

*Potential refractive index will be more explicitly defined later. It is a quantity defined such that it is invariant when its air parcel undergoes adiabatic change.

Subsidence within an air mass can be the result of descent of the air mass due to topography or it can result from divergence in the lower levels. One classical example of topographic subsidence occurs when air from the high desert interior of the western United States flows down toward the coast of southern California and out over the sea. A strong low-level inversion forms, often surface based, in the air over the coastal water. A very strong refractive gradient results from the temperature inversion and also from the evaporation of moisture into the dry continental air. Spectacular refraction of both optical and radio waves then occurs and, when this condition is coupled with a strong trade wind inversion, it is not uncommon for VHF transmissions from the United States west coast to be received in Hawaii. Optical refraction is even

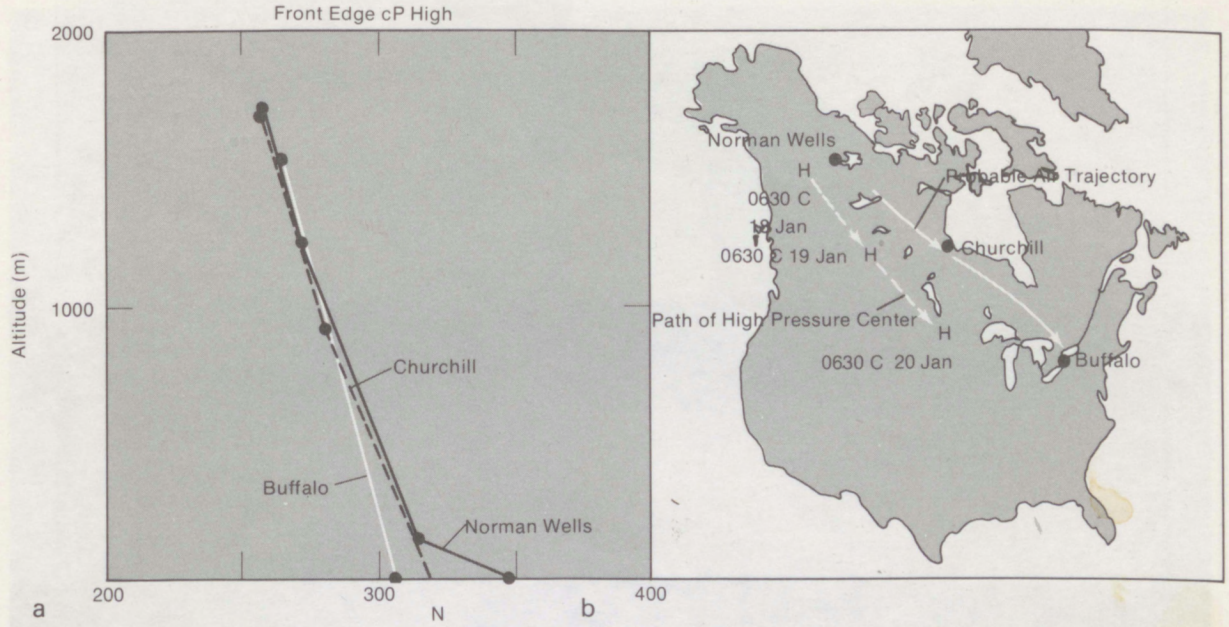

Frame 4a, b **Modification of the surface layers of an air mass as it moves southward along a trajectory shown by the solid arrows on the map at the right. (Adapted from Plank, 1952)**

more vividly apparent. Images of islands and ships beyond the geometrical horizon are often seen over paths with several combinations of atmospheric and oceanic reflection as shown in Fig. 6. Similar cases of topographic subsidence occur over the coastal waters off Alaska.

A somewhat different kind of topographic subsidence is common on the eastern slope of the Rocky Mountains and the adjacent plains. This subsidence occurs when a deep, wide-spread westerly circulation dominates the area. When enhanced by a surface-based radiation inversion, it can produce severe air pollution in the Denver area as well as strong radio refraction. An example of the refractive index distribution during this subsidence condition (without the surface radiation duct) is shown by the Denver sounding in Fig. 7. In spite of subsidence, solar heating often creates a nearly adiabatic layer near the ground. Because the humidity is low in this air mass, the potential refractive index gradient can be very small and the refractive index variance is then also small (Bean, 1968).

Another type of subsidence occurs within an air mass due to divergence. This commonly occurs in a southward moving air mass having an anticyclonic circulation pattern. To see this,

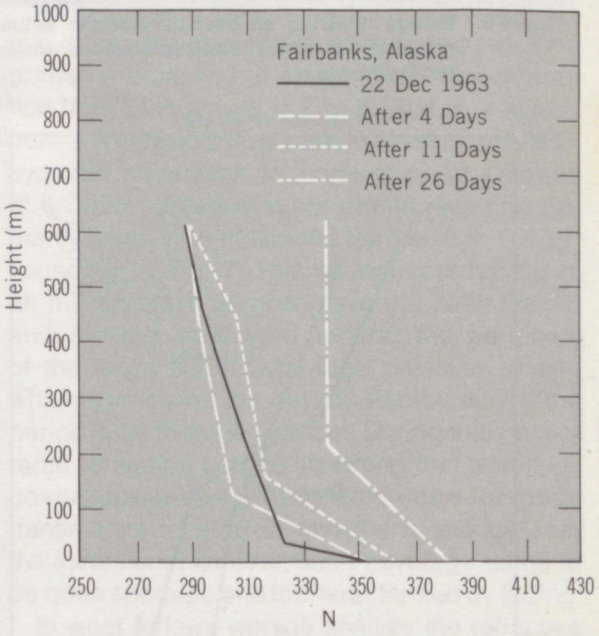

Figure 5. **Modification of the surface layers of an air mass in its source region as radiational cooling of the underlying surface proceeds.**

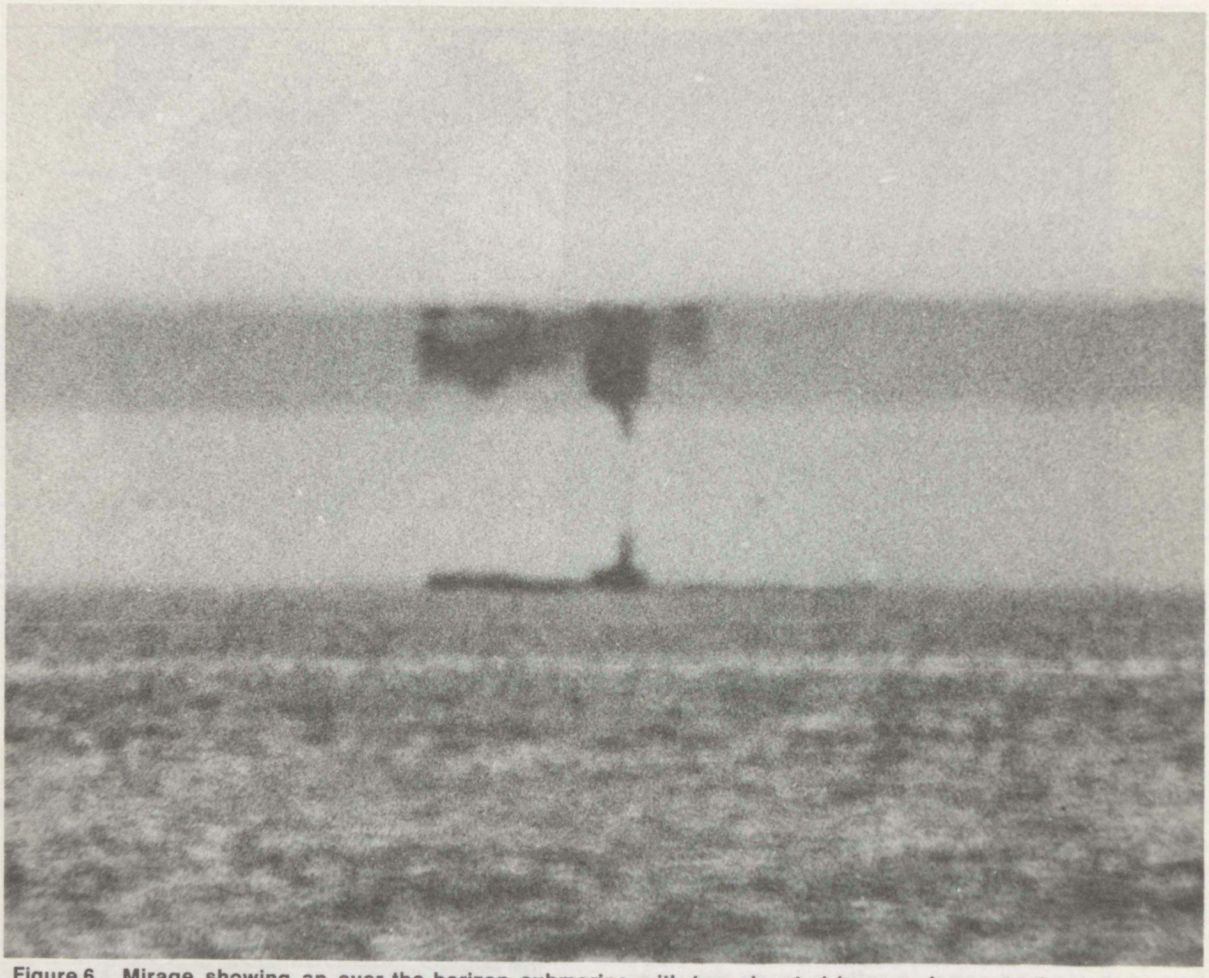

Figure 6. Mirage showing an over-the-horizon submarine with two elevated images demonstrating intense refraction of optical and radio waves under conditions of strong subsidence off the coast of southern California.

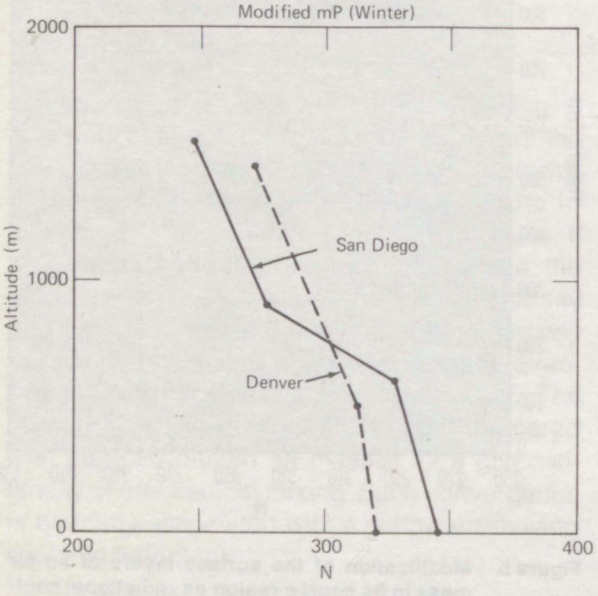

Figure 7. Refractive index N distribution resulting from two kinds of subsidence in different climatic regimes.

consider a column of air whose rotation about a vertical axis is given by the angular velocity ω, chosen positive for cyclonic rotation. We define ω to be the angular velocity *relative* to the surface of the earth. The angular velocity of a point on the earth's surface beneath the air parcel is given by $\Omega \sin \phi$, where Ω is the angular velocity of rotation of the earth about its axis and ϕ is latitude. It is counterclockwise in the northern hemisphere. Suppose we represent the air column as a cylinder of height H and radius R. Its total angular velocity will then be $\omega + \Omega \sin \phi$, and if its angular momentum is conserved we may write

$$(\omega + \Omega \sin \phi)\, R^2 = \text{constant}.$$

Assuming the mass within the cylinder to be also conserved while it undergoes divergence or

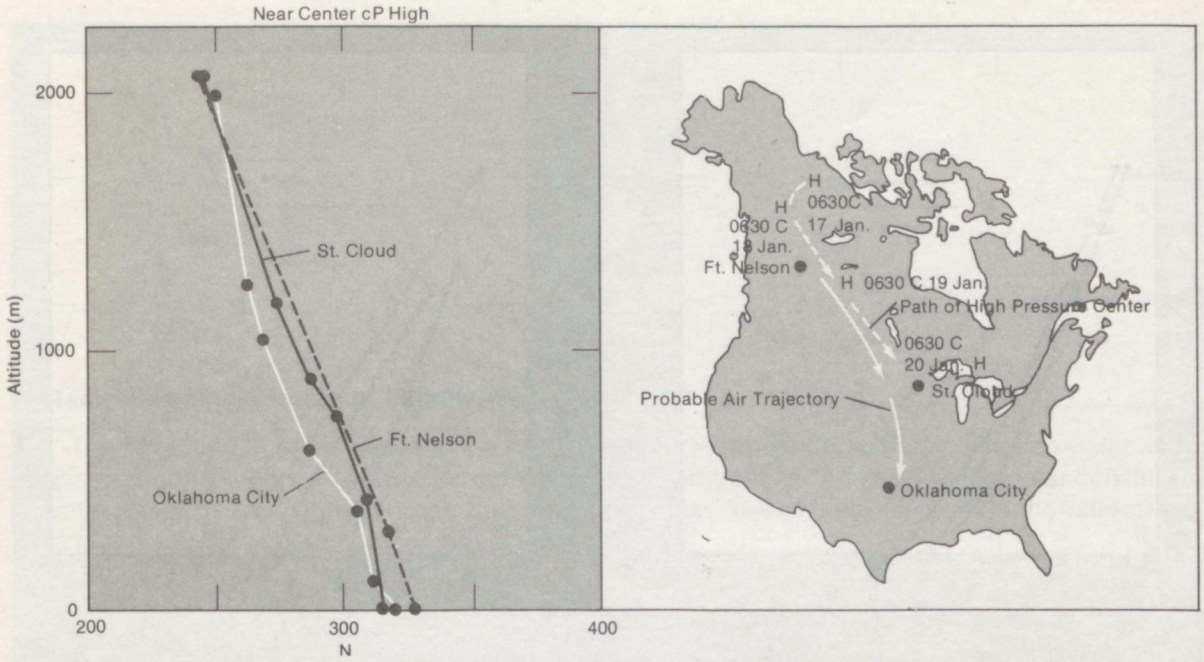

Figure 8. Height distribution of radio refractive index N in an air mass which is subsiding as it moves southward anticyclonically along the trajectory shown by the solid arrows on the map to the right.

convergence, its volume will then be conserved if density changes are ignored. Therefore lateral convergence will be compensated by vertical stretching and divergence by vertical shrinking (subsidence). Under these assumptions, the volume is

$$V = \pi R^2 H,$$

so $(\omega + \Omega \sin \phi) / H$ = constant. Substitution of the Coriolis parameter $f = 2\Omega \sin \phi$ in place of the angular velocity of the point on the earth's surface and substitution of the vorticity $\zeta = 2\omega$ in place of angular velocity of the column relative to the earth's surface, gives

$$\frac{\zeta + f}{H} = \text{constant}$$

where ζ is positive for cyclonic curvature of the airflow. This is one form of Rossby's vorticity equation. It is immediately apparent that decreasing absolute vorticity leads to shrinkage of the air column. The following conclusions may be stated:

1) Decreasing vorticity (increasing anticyclonic circulation) at a given latitude leads to subsidence within the air mass and vice versa.
2) In the absence of lateral convergence or divergence, increasing vorticity results from a northerly (equatorward) flow in the northern hemisphere or a southerly flow in the southern hemisphere.
3) If vorticity in the air mass is conserved, subsidence (i.e., divergence) occurs in a northerly (equatorward) flow in the northern hemisphere or a southerly flow in the southern hemisphere.

An example of the modification of radio refractive index due to air mass subsidence resulting primarily from 1), but also with some contribution from 3) is shown in Fig. 8. That is, it results from a southward flow pattern in which the anticyclonic circulation is increasing. An example of a radio refractive index profile resulting primarily from 3) is illustrated by the "San Diego" sounding in Fig. 7. This sounding is typical of an mP air mass originating in the north Pacific and moving southward around the periphery of the large subtropical high pressure system which dominates the eastern Pacific during the period June through October. During this period, radio refraction can be so strong that television coverage can be greatly enhanced for these transmitters located at elevations just beneath the inversion. However, such coverage tends to be quite sporadic and is characterized by fading.

In what follows we will analyze the refractive structure of air masses and frontal surfaces, and examine some of the implications of this refractive structure on the propagation of short radio waves.

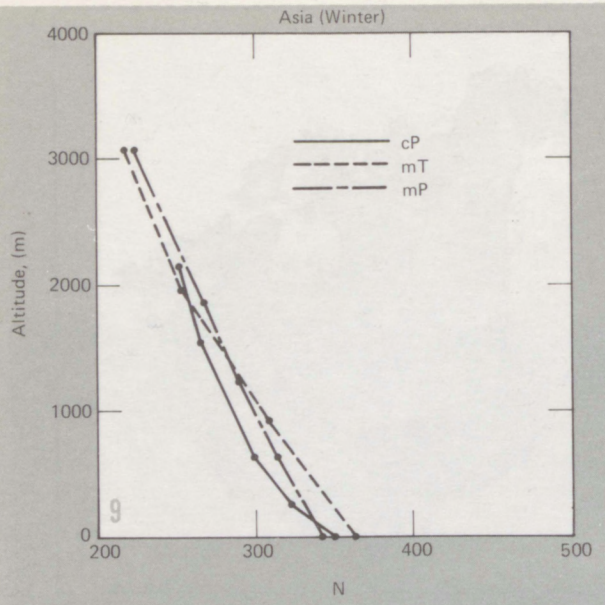

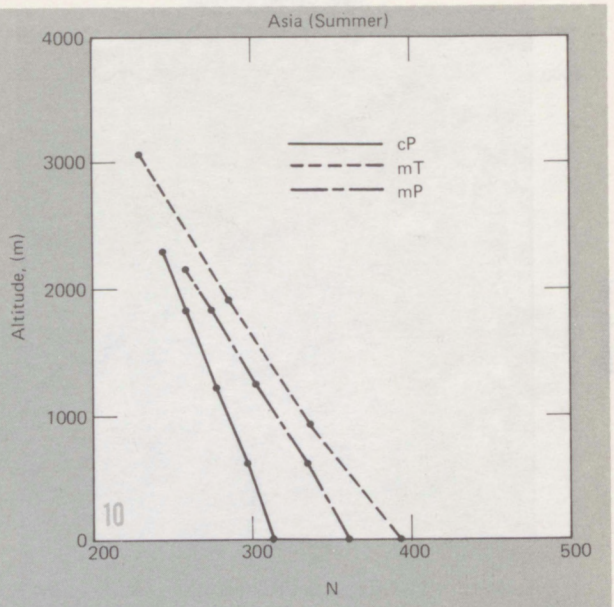

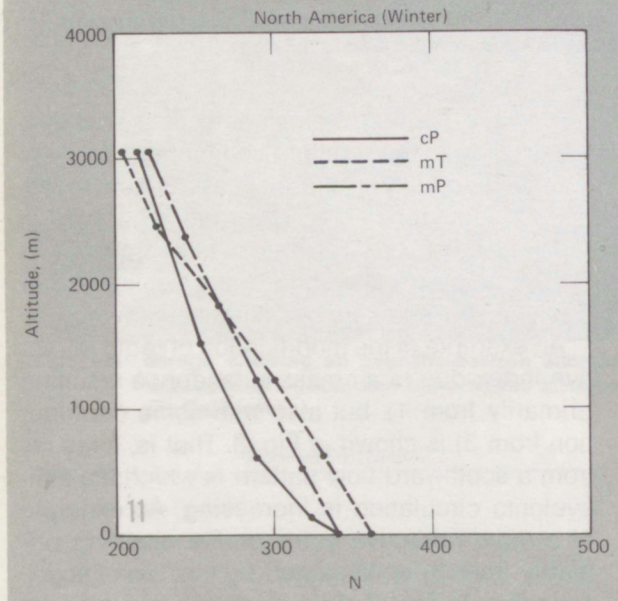

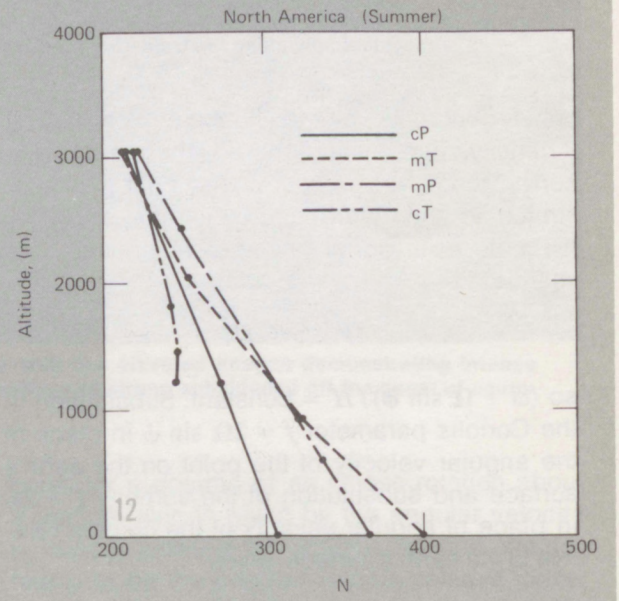

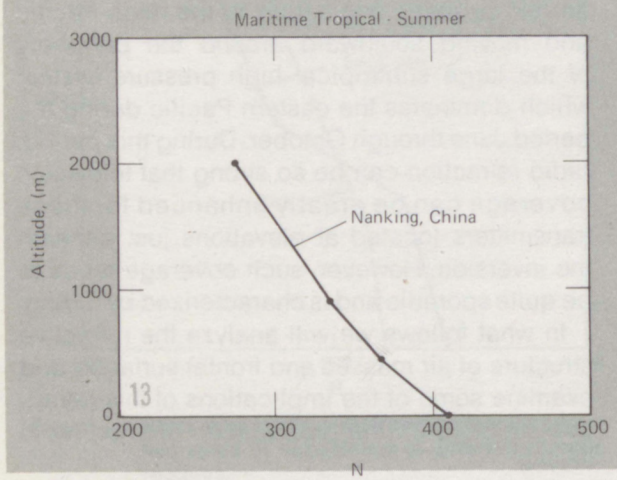

Figure 9. **Typical radio refractive index N distribution in some North American air masses (Asian winter).**

Figure 10. **Typical radio refractive index N distribution in some North American air masses (Asian summer).**

Figure 11. **Typical radio refractive index N distribution in some North American air masses (winter).**

Figure 12. **Typical radio refractive index N distribution in some North American air masses (summer).**

Figure 13. **Height distribution of radio refractive index in maritime tropical air mass at Nanking, China (summer).**

Radio Refractive Index at Microwave Frequencies

The refraction of radio waves in the non-ionized atmosphere depends on both non-polar and polar gaseous constituents. However, for comparable concentrations, the effect of the polar constituent, i.e. water vapor, is much greater than that of the non-polar. The expression relating the refractive index m to the various meteorological measurables is:

$$(n-1) \times 10^6 = K_1 \frac{p_d}{T} + K_2 \frac{e}{T} + K_3 \frac{e}{T^2} + K_4 \frac{p_c}{T} \tag{1a}$$

where K_1, K_2, K_3 and K_4 are constants, T is absolute temperature, p_d is partial pressure of the dry air constituents, e is partial pressure of water vapor and p_c is partial pressure of carbon dioxide. The first and fourth terms represent the effects of non-polar constituents and the second and third represent the effects of polar constituents. A summary of the values of K found by various workers has been given by Bean and Dutton (1966). Here, we simply adopt the values of Smith and Weintraub. If we define $N = (n-1) \times 10^6$, this gives

$$N = 77.6 \frac{p_d}{T} + 72 \frac{e}{T} + 3.75 \times 10^5 \frac{e}{T^2} \tag{1b}$$

where p_d and e are in millibars. Because total pressure p is the easy quantity to measure, substitute $p_d = p - e$ and (1b) becomes

$$N = 77.6 \frac{p}{T} - 5.6 \frac{e}{T} + 3.75 \times 10^5 \frac{e}{T^2}.$$

Therefore, for $T \simeq 300$

$$N = 77.6 \frac{p}{T} + \frac{e}{T^2}(3.75 \times 10^5 - 5.6\,T) \simeq 77.6 \frac{p}{T} + 3.73 \times 10^5 \frac{e}{T^2} \tag{1c}$$

which is commonly written in the form

$$N = \frac{77.6}{T}\left[p + \left(\frac{4810\,e}{T}\right)\right]. \tag{1d}$$

Typical refractive index height distributions in North America and Asia are shown in Figs. 9, 10, 11, 12, and 13, modified from Plank (1952). Refractive index distributions at specific locations in the United States, calculated from temperature and humidity profiles published by Showalter (1939), are shown in Figs. 14 to 22.

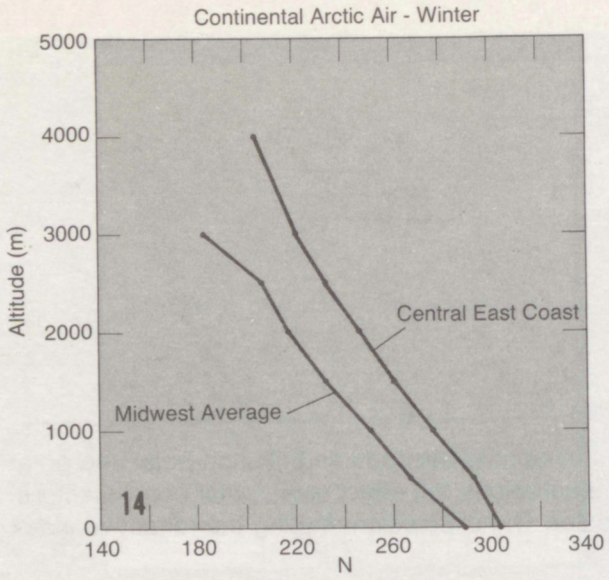

Figure 14. Height distribution of radio refractive index in various North American air masses measured at the locations and seasons indicated.

Figure 15. Height distribution of radio refractive index in various North American air masses measured at the locations and seasons indicated.

Figure 16. Height distribution of radio refractive index in various North American air masses measured at the locations and seasons indicated.

Figure 17. Height distribution of radio refractive index in various North American air masses measured at the locations and seasons indicated.

Figure 18. Height distribution of radio refractive index in various North American air masses measured at the locations and seasons indicated.

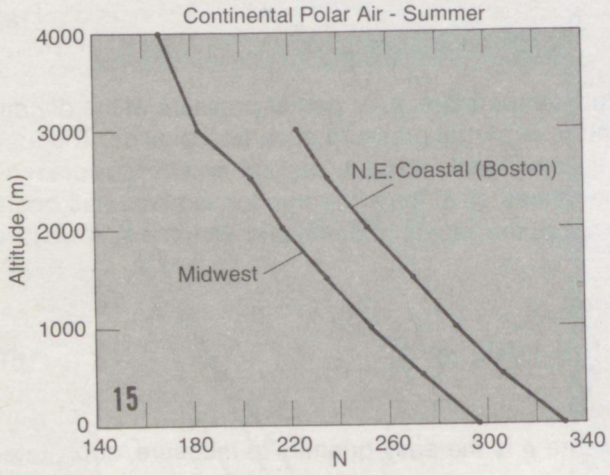

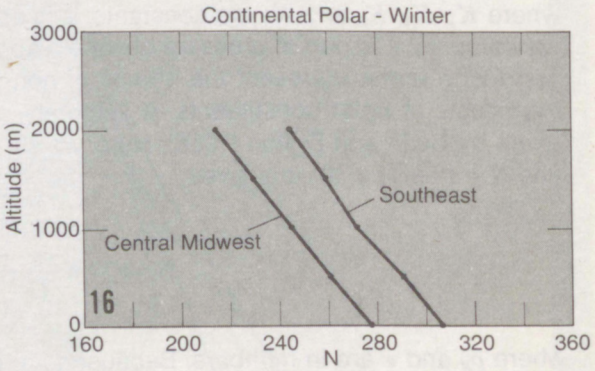

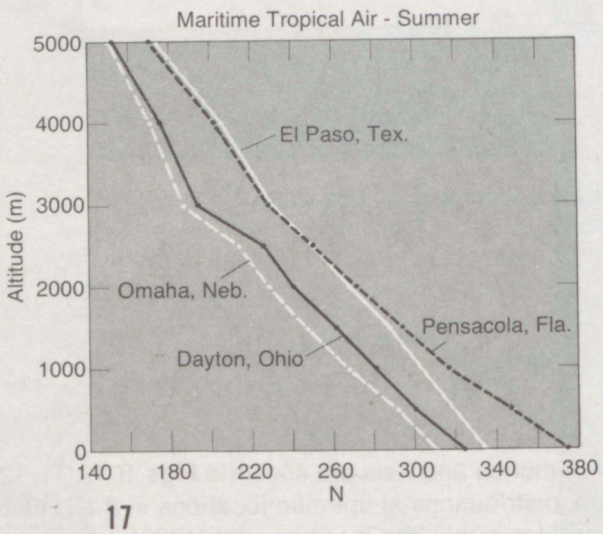

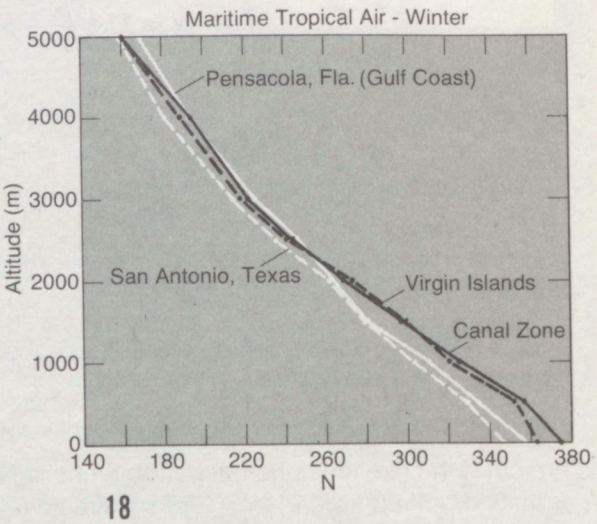

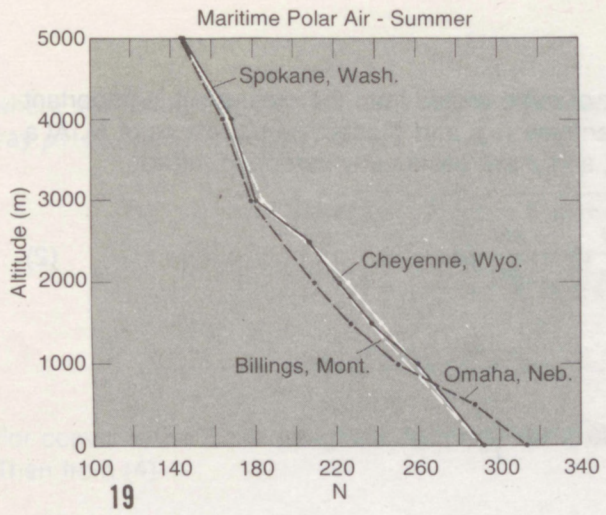

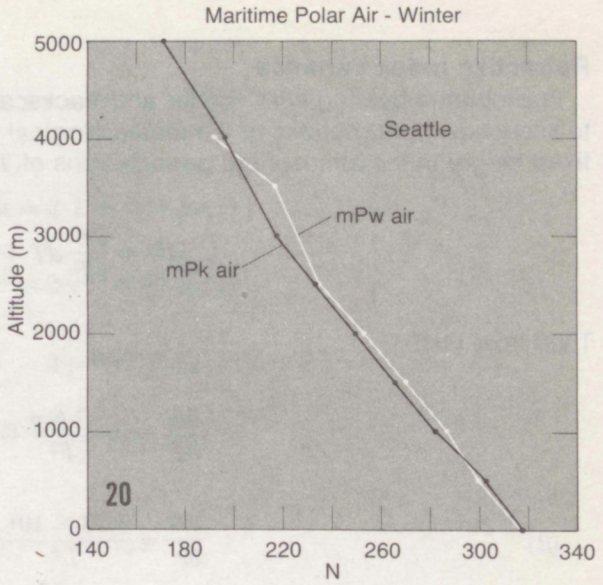

Figure 19. **Height distribution of radio refractive index in various North American air masses measured at the locations and seasons indicated.**

Figure 20. **Height distribution of radio refractive index in various North American air masses measured at the locations and seasons indicated.**

Figure 21. **Height distribution of radio refractive index in various North American air masses measured at the locations and seasons indicated.**

Figure 22. **Height distribution of radio refractive index in various North American air masses measured at the locations and seasons indicated.**

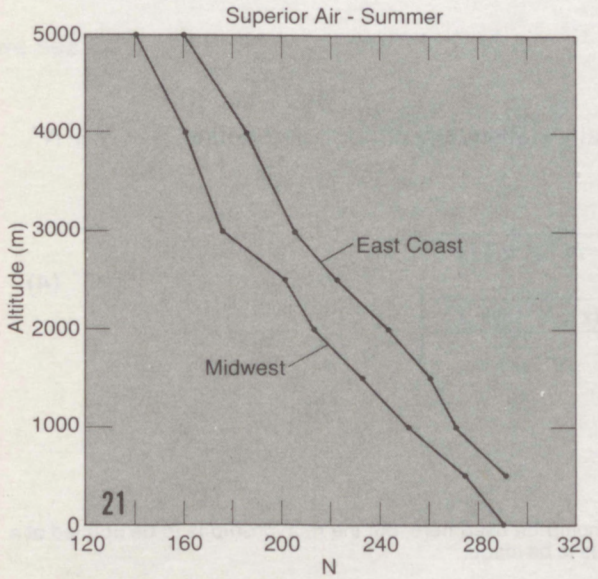

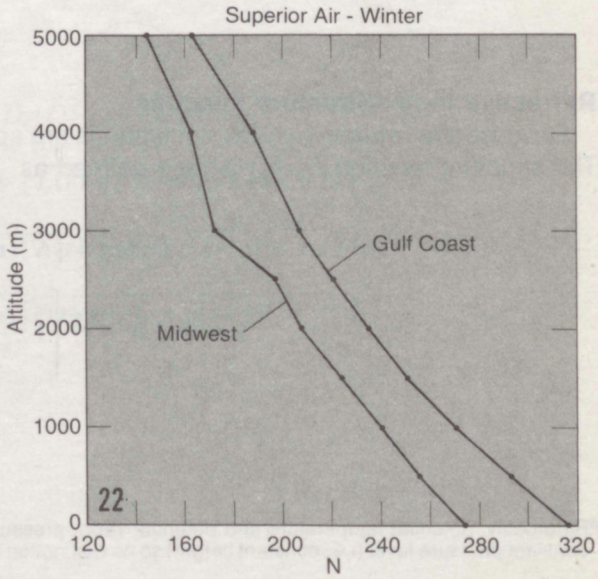

Refractive Index Variance

In problems dealing with scatter and backscatter of radio waves from the clear air it is important to know how perturbations of the meteorological quantities e, p and T affect perturbations of N. At a fixed height in the atmosphere perturbations of T, e, and p are essentially independent, so*

$$dN = \frac{\partial N}{\partial T}\, dT + \frac{\partial N}{\partial e}\, de + \frac{\partial N}{\partial p}\, dp. \tag{2}$$

Then from (1d)

$$\frac{\partial N}{\partial T} = -\frac{77.6\, p}{T^2} - 7.46 \times 10^5 \frac{e}{T^3} = -a$$

$$\frac{\partial N}{\partial e} = \frac{3.73 \times 10^5}{T^2} = b$$

$$\frac{\partial N}{\partial p} = \frac{77.6}{T} = c$$

which define the quantities a, b, and c.

Using primes to indicate dN, dT, dp, and de, (2) can be written

$$N' = -aT' + be' + cp'$$

and the variance of refractive index is related to the variance of the meteorological quantities by

$$\overline{N'^2} = a^2\,\overline{T'^2} + b^2\,\overline{e'^2} + c^2\,\overline{p'^2} - 2ab\,\overline{T'e'} - 2ac\,\overline{T'p'} + 2bc\,\overline{p'e'}. \tag{3}$$

The possible importance of the term in $\overline{T'e'}$, when temperature and humidity fluctuations are correlated, was pointed out and evaluated by Gossard (1960).

Refractive Index Structure Function

Suppose the refractive index fluctuations are spatially statistically uniform and define $N = \overline{N} + N'$. The structure function $D_N(\ell)$ is then defined as

$$\begin{aligned} D_N(\ell) &= \overline{[N'(r) - N'(r+\ell)]^2} \\ &= 2\,\overline{N'^2(r)} \left[1 - \frac{\overline{N'(r)\, N'(r+\ell)}}{\overline{N'^2(r)}} \right], \end{aligned} \tag{4}$$

*Rigorously, potential temperature and potential vapor pressure should be used here, but the relationship is to be applied at a constant pressure level (i.e., constant height) so no distinction needs to be made.

where we recognize the last term inside the brackets as just the spatial auto-correlation function, say $\rho_N(\ell)$. Then similarly

$$D_T(\ell) = \overline{[T'(r) - T'(r+\ell)]^2} = 2\,\overline{T'^2(r)}\,[1\text{-}\rho_T(\ell)]$$

$$D_e(\ell) = \overline{[e'(r) - e'(r+\ell)]^2} = 2\,\overline{e'^2(r)}\,[1\text{-}\rho_e(\ell)]$$

$$D_p(\ell) = \overline{[p'(r) - p'(r+\ell)]^2} = 2\,\overline{p'^2(r)}\,[1\text{-}\rho_p(\ell)]$$

For convenience we redesignate $N'(r) = N_1$, $N'(r+\ell) = N_2$, etc.
Then from (4)

$$D_N(\ell) = \overline{N_1^2} + \overline{N_2^2} - 2\,\overline{N_1 N_2}. \tag{5}$$

From our assumptions of statistical uniformity and Eq (3)

$$\overline{N_1^2} = \overline{N_2^2} = a^2\,\overline{T'^2} + b^2\,\overline{e'^2} + c^2\,\overline{p'^2} - 2\,ab\,\overline{T'e'} - 2\,ac\,\overline{T'p'} + 2\,bc\,\overline{p'e'}.$$

Also assuming $\overline{T_1 T_2} = \overline{T_2 T_1}$, etc.

$$\overline{N_1 N_2} = a^2\,\overline{T^1 T^2} + b^2\,\overline{e_1 e_2} + c^2\,\overline{p_1 p_2} - 2\,ab\,\overline{T_1 e_2} - 2\,ac\,\overline{T_1 p_2} + 2\,cb\,\overline{e_1 p_2}.$$

Recalling that $D_T(\ell)$, $D_e(\ell)$, $D_p(\ell)$ are of the same form as (5), e.g.,

$$D_T(\ell) = \overline{T_1^2} + \overline{T_2^2} - 2\,\overline{T_1 T_2},$$

we see that

$$\begin{aligned} D_N(\ell) = a^2\,D_T(\ell) + b^2\,D_e(\ell) + c^2\,D_p(\ell) \\ - 2ab\,[\overline{T(r)\,e(r)} - \overline{T(r)\,e(r+\ell)}] \\ - 2ac\,[\overline{T(r)\,p(r)} - \overline{T(r)\,p(r+\ell)}] \\ + 2bc\,[\overline{e(r)\,p(r)} - \overline{e(r)\,p(r+\ell)}]\,. \end{aligned}$$

Therefore:

$$D_N(\ell) = a^2 D_T(\ell) + b^2 D_e(\ell) + c^2 D_p(\ell) - 2ab\, D_{Te}(\ell) - 2ac\, D_{Tp}(\ell) + 2cb\, D_{ep}(\ell) \qquad (6)$$

where

$$D_N(\ell) = 2\,\overline{N'^2}\,[1\text{-}\rho_N(\ell)]$$

$$D_T(\ell) = 2\,\overline{T'^2}\,[1\text{-}\rho_T(\ell)]$$

$$D_e(\ell) = 2\,\overline{e'^2}\,[1\text{-}\rho_e(\ell)]$$

$$D_p(\ell) = 2\,\overline{p'^2}\,[1\text{-}\rho_p(\ell)]$$

$$D_{Te}(\ell) = 2\,\overline{T'e'}\,[1\text{-}\rho_{Te}(\ell)]$$

$$D_{Tp}(\ell) = 2\,\overline{T'p'}\,[1\text{-}\rho_{Tp}(\ell)]$$

$$D_{ep}(\ell) = 2\,\overline{e'p'}\,[1\text{-}\rho_{ep}(\ell)]$$

Table 2.

CONTINENTAL POLAR-WINTER

Oklahoma City									
Ht.	a	b	c	a^2	b^2	c^2	2ab	2ac	2bc
0	1.09	5.19	0.29	1.19	26.9	0.08	11.3	0.63	3.00
500	1.02	5.17	0.29	1.05	26.7	0.08	10.6	0.59	2.98
1000	0.96	5.15	0.29	0.92	26.5	0.08	9.88	0.55	2.97
1500	0.90	5.19	0.29	0.81	26.9	0.08	9.37	0.52	3.00
2000	0.84	5.15	0.29	0.71	26.5	0.08	8.70	0.49	2.97

and the ρ's are the spatial auto- and cross-correlation functions. They are, of course, normalized, so the variance and covariance appear as factors outside the brackets.

Within the inertial subrange we can express the structure function $D(\ell)$ in terms of the structure constant C^2, e.g.,

$$D_N(\ell) = C_N^2 \, \ell^{2/3}$$

So, for any given ℓ,

$$C_N^2 = a^2 C_T^2 + b^2 C_e^2 + c^2 C_p^2 - 2ab \, C_{Te}^2 - 2ac \, C_{Tp}^2 + 2bc \, C_{ep}^2. \qquad (6a)$$

It is reasonable to suppose that the quantity in brackets, in the expressions for D, is very nearly the same for all D, so all D (or C^2) can be expressed in terms of one (say C_T^2) by simply multiplying by the ratio of their variances or covariances, and the ratios of the factors a^2, b^2, c^2, ab, ac, cb multiplying the appropriate terms. The values of the coefficients in Eq. (6) and (6a), for a variety of air masses and locations, are shown in Tables 2 through 9.

Table 3.

MARITIME POLAR-WINTER

Seattle									
Ht.	a	b	c	a^2	b^2	c^2	2ab	2ac	2bc
0	1.27	4.76	0.28	1.62	22.6	0.08	12.1	0.71	2.63
500	1.22	4.84	0.28	1.49	23.5	0.08	11.8	0.68	2.71
1000	1.13	4.93	0.28	1.28	24.3	0.08	11.2	0.64	2.78
1500	1.06	5.05	0.28	1.13	25.5	0.08	10.7	0.61	2.88
2000	1.00	5.15	0.29	1.00	26.6	0.08	10.3	0.58	2.97
2500	0.29	2.01	−0.18	0.08	4.03	0.03	1.16	−0.10	0.72
3000	0.86	5.42	0.30	0.75	29.4	0.09	9.43	0.51	3.21
4000	0.77	5.73	0.30	0.60	32.8	0.09	8.87	0.47	3.48
5000	0.70	6.13	0.31	0.49	37.6	0.10	8.61	0.44	3.86

Table 4.

MARITIME TROPICAL-WINTER

Ht.	a	b	c	a^2	b^2	c^2	2ab	2ac	2bc
Canal Zone									
0	1.64	4.21	0.26	2.69	17.7	0.07	13.8	0.85	2.19
500	1.56	4.28	0.26	2.44	18.4	0.07	13.4	0.82	2.25
1000	1.41	4.37	0.27	1.98	19.1	0.07	12.3	0.75	2.32
1500	1.26	4.46	0.27	1.60	19.9	0.07	11.3	0.68	2.39
2000	1.12	4.52	0.27	1.25	20.4	0.07	10.1	0.60	2.44
2500	0.99	4.59	0.27	0.99	21.0	0.07	9.11	0.54	2.49
3000	0.89	4.66	0.27	0.79	21.7	0.07	8.30	0.48	2.56
4000	0.76	4.81	0.28	0.58	23.1	0.08	7.33	0.42	2.67
5000	0.61	4.99	0.28	0.37	24.9	0.08	6.12	0.35	2.82
Pensacola									
0	1.54	4.36	0.26	2.37	19.0	0.07	13.4	0.82	2.31
500	1.42	4.40	0.27	2.02	19.4	0.07	12.5	0.76	2.35
1000	1.32	4.50	0.27	1.74	20.2	0.07	11.9	0.71	2.43
1500	1.16	4.60	0.27	1.35	21.2	0.07	10.7	0.63	2.51
2000	1.09	4.69	0.27	1.19	22.0	0.08	10.2	0.60	2.58
2500	1.01	4.81	0.28	1.01	23.1	0.08	9.69	0.56	2.68
3000	0.92	4.91	0.28	0.85	24.1	0.08	9.04	0 52	2.77
4000	0.76	4.91	0.28	0.58	24.1	0.08	7.46	0.43	2.77
5000	0.68	5.37	0.29	0.47	28.9	0.09	7.36	0.40	3.16

Table 5. SUPERIOR AIR-WINTER

Oklahoma City									
Ht.	a	b	c	a^2	b^2	c^2	2ab	2ac	2bc
0	1.06	4.76	0.28	1.12	22.7	0.08	10.1	0.59	2.64
500	0.99	4.66	0.27	0.97	21.7	0.07	9.20	0.54	2.56
1000	0.92	4.59	0.27	0.85	21.1	0.07	8.45	0.50	2.50
1500	0.86	4.61	0.27	0.73	21.3	0.07	7.91	0.47	2.52
2000	0.80	4.73	0.28	0.64	22.4	0.08	7.56	0.44	2.61
2500	0.75	4.86	0.28	0.57	23.6	0.08	7.31	0.42	2.72
3000	0.69	4.89	0.28	0.48	24.0	0.08	6.77	0.39	2.75
4000	0.63	5.25	0.29	0.39	27.6	0.08	6.59	0.36	3.06
5000	0.56	5.54	0.30	0.32	30.7	0.09	6.26	0.34	3.32
Pensacola									
0	–	–	–	–	–	–	–	–	–
500	1.15	4.51	0.27	1.33	20.3	0.07	10.4	0.62	2.43
1000	1.06	4.65	0.27	1.12	21.7	0.07	9.8	0.58	2.55
1500	0.95	4.74	0.28	0.91	22.5	0.08	9.06	0.53	2.63
2000	0.89	4.79	0.28	0.79	23.0	0.08	8.53	0.49	2.67
2500	0.83	4.86	0.28	0.70	23.6	0.08	8.16	0.47	2.72
3000	0.79	4.96	0.28	0.63	24.6	0.08	7.85	0.45	2.81
4000	0.71	5.15	0.29	0.50	26.6	0.08	7.29	0.41	2.97
5000	0.63	5.40	0.29	0.40	29.2	0.08	6.83	0.37	3.19

The pressure fluctuations are typically more than an order of magnitude smaller than the water vapor or temperature fluctuations, and c^2 and products of c with a and b are typically orders of magnitude less than a^2, b^2 or ab. Consequently, the important terms are

$$C_N^2 \simeq a^2 C_T^2 + b^2 C_e^2 - 2ab\, C_{Te}^2 \tag{7}$$

where

$$C_e^2 = \frac{\overline{e'^2}}{\overline{T'^2}}\, C_T^2$$

$$C_{Te}^2 = \frac{\overline{T'e'}}{\overline{T'^2}}\, C_T^2 .$$

Table 6.

CONTINENTAL POLAR-SUMMER

Omaha									
Ht.	a	b	c	a^2	b^2	c^2	2ab	2ac	2bc
0	1.22	4.42	0.27	1.48	19.5	0.07	10.8	0.65	2.36
500	1.25	4.35	0.27	1.57	18.9	0.07	10.9	0.66	2.31
1000	1.14	4.42	0.27	1.29	19.5	0.07	10.0	0.61	2.36
1500	1.06	4.51	0.27	1.11	20.3	0.07	9.53	0.57	2.43
2000	0.98	4.59	0.27	0.96	21.1	0.07	9.04	0.54	2.50
2500	0.91	4.67	0.27	0.83	21.8	0.07	8.52	0.50	2.57
3000	0.89	4.70	0.28	0.79	22.1	0.08	8.34	0.49	2.59
4000	–	–	–	–	–	–	–	–	–
5000	–	–	–	–	–	–	–	–	–

If we presume it is possible to acquire information about the height distribution of C_T^2 in a variety of air masses, a convenient form of (7) is

$$\frac{C_N^2}{C_T^2} \simeq a^2 + b^2 \frac{C_e^2}{C_T^2} - 2ab \frac{C_{Te}^2}{C_T^2}$$

or

$$\frac{C_N^2}{C_T^2} \simeq a^2 + b^2 \frac{\overline{e'^2}}{\overline{T'^2}} - 2ab \frac{\overline{e'T'}}{\overline{T'^2}}. \tag{8}$$

To proceed further with the analysis of C_N^2, having only mean profile data from many air masses, requires additional assumptions. One assumption with some physics to support it is the classical mixing length concept, in which one assumes that

$$e_p', \theta' = L \frac{d(\overline{e_p}, \overline{\theta})}{dz}$$

where L is a mechanical mixing length, analogous to the molecular mean free path in Brownian diffusion, and e_p and θ are the potential vapor pressure and potential temperature, respectively. They are the values of e and T that a parcel of air would have if it were taken adiabatically to some reference pressure without change of state. The reference pressure is usually 1000 *mb*, so $\theta = T\ (1000/p)^{0.286}$ and $e_p = e\ (1000/p)$. *To illustrate, suppose the line segment in the schematic at right represents a portion of the height profile of potential temperature. If an air parcel, A, with potential temperature $\bar{\theta}_2$ is mixed downward a distance L, it will cause a perturbation of θ at that level equal to $L\ d\theta/dz$. In like manner, if an air parcel, B, with potential temperature $\bar{\theta}_1$ is mixed upward it will cause a similar perturbation in θ at its new level.* The same arguments apply to e_p; so, if the same mechanical mixing length applies to θ and e_p

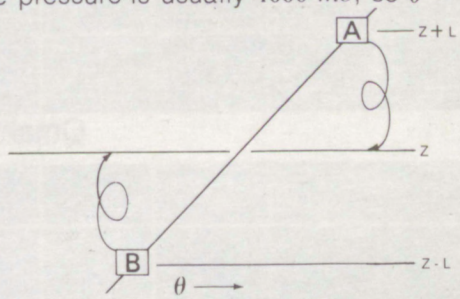

$$\left(\frac{1000}{p}\right)^{1.43} \frac{\overline{e'^2}}{\overline{T'^2}} = \frac{\overline{e_p'^2}}{\overline{\theta'^2}} = \frac{(d\bar{e}/dz)^2}{(d\bar{\theta}/dz)^2} = \frac{\Delta\bar{e}_p}{\Delta\bar{\theta}^2} \tag{9}$$

and

$$\left(\frac{1000}{T}\right)^{0.714} \frac{\overline{e'T'}}{\overline{T'^2}} = \frac{\overline{e_p'\theta'}}{\overline{\theta'^2}} \cong \frac{\Delta\bar{e}_p}{\Delta\bar{\theta}} \tag{10}$$

From mean profile data in various air masses, the terms on the right-hand side of (8) can be estimated and thus an estimate of C_N^2/C_T^2 can be obtained.

If the quantities θ and e_p are used instead of T and e, Eq. (1d) yields the potential refractive index referred to earlier. It will be designated ϕ.

Table 7.

MARITIME POLAR-SUMMER

Spokane									
Ht.	a	b	c	a^2	b^2	c^2	2ab	2ac	2bc
0	1.18	4.48	0.27	1.40	20.0	0.07	10.6	0.63	2.41
500	–	–	–	–	–	–	–	–	–
1000	1.05	4.35	0.27	1.09	18.9	0.07	9.11	0.55	2.31
1500	0.94	4.35	0.27	0.89	18.9	0.07	8.22	0.50	2.31
2000	0.88	4.54	0.27	0.78	20.7	0.07	8.03	0.48	2.46
2500	0.83	4.68	0.28	0.69	21.9	0.08	7.80	0.46	2.57
3000	0.78	4.79	0.28	0.60	22.9	0.08	7.44	0.43	2.67
4000	0.68	5.15	0.29	0.46	26.5	0.08	7.04	0.39	2.97
5000	0.58	5.29	0.29	0.34	28.0	0.08	6.14	0.34	3.09
Omaha									
0	1.32	4.26	0.26	1.74	18.0	0.07	11.2	0.69	2.22
500	1.19	4.23	0.26	1.41	17.9	0.07	10.1	0.62	2.21
1000	0.98	4.26	0.26	0.96	18.1	0.07	8.38	0.52	2.23
1500	0.87	4.41	0.27	0.76	19.5	0.07	7.72	0.46	2.36
2000	0.80	4.52	0.27	0.64	20.4	0.07	7.25	0.43	2.44
2500	0.83	4.72	0.28	0.68	22.3	0.08	7.81	0.46	2.61
3000	0.77	4.84	0.28	0.58	23.4	0.08	7.41	0.43	2.70
4000	0.67	5.05	0.29	0.44	25.5	0.08	6.74	0.38	2.88
5000	0.58	5.29	0.29	0.33	28.0	0.08	6.12	0.34	3.09

Table 8.

MARITIME TROPICAL-SUMMER

Ht.	a	b	c	a^2	b^2	c^2	2ab	2ac	2bc
Pensacola									
0	1.65	4.23	0.26	2.70	17.9	0.07	13.9	0.86	2.21
500	1.50	4.22	0.26	2.24	17.8	0.07	12.6	0.78	2.20
1000	1.35	4.30	0.26	1.82	18.5	0.07	11.6	0.71	2.27
1500	1.24	4.40	0.27	1.54	19.4	0.07	10.9	0.66	2.35
2000	1.13	4.49	0.27	1.28	20.2	0.07	10.2	0.61	2.42
2500	1.04	4.58	0.27	1.08	20.9	0.07	9.52	0.56	2.49
3000	0.94	4.67	0.27	0.88	21.8	0.07	8.79	0.52	2.56
4000	0.82	4.88	0.28	0.66	23.8	0.08	7.97	0.46	2.74
5000	0.69	5.09	0.29	0.48	25.9	0.08	7.07	0.40	2.92
Omaha									
0	1.31	4.21	0.26	1.71	17.7	0.07	11.0	0.68	2.20
500	1.22	4.15	0.26	1.48	17.3	0.07	10.1	0.63	2.15
1000	1.10	4.13	0.26	1.20	17.1	0.07	9.06	0.56	2.13
1500	1.00	4.21	0.26	1.01	17.7	0.07	8.46	0.52	2.19
2000	0.93	4.33	0.26	0.87	18.7	0.07	8.07	0.49	2.28
2500	0.87	4.45	0.26	0.76	19.8	0.07	7.78	0.47	2.39
3000	0.81	4.56	0.27	0.66	20.8	0.07	7.41	0.44	2.47
4000	0.69	4.80	0.28	0.48	23.0	0.08	6.66	0.38	2.67
5000	0.61	5.09	0.29	0.37	25.9	0.08	6.18	0.35	2.92

Table 9.

SUPERIOR AIR-SUMMER Omaha									
Ht.	a	b	c	a^2	b^2	c^2	2ab	2ac	2bc
0	1.17	4.12	0.26	1.39	16.9	0.07	9.67	0.61	2.12
500	1.12	4.02	0.26	1.25	16.2	0.07	9.01	0.57	2.05
1000	1.00	4.06	0.26	1.00	16.3	0.07	8.13	0.51	2.08
1500	0.92	4.18	0.26	0.85	17.5	0.07	7.73	0.48	2.17
2000	0.82	4.29	0.26	0.67	18.5	0.07	7.04	0.43	2.26
2500	0.76	4.40	0.27	0.58	19.4	0.07	6.72	0.41	2.34
3000	0.72	4.54	0.27	0.52	20.7	0.07	6.53	0.39	2.46
4000	–	4.80	0.28	–	23.0	0.08	–	–	2.67
5000	0.54	5.08	0.29	0.30	25.8	0.08	–	–	2.90

Discussion

Four types of plots are included in Figs. 9 to 43. The first set of plots (Figs. 9-22) shows the distribution of N with height for summer and winter in the various air masses for selected locations in the Western Hemisphere. This information is mainly of value in calculating the refractive properties of the troposphere and estimating the variability of the effective radio horizon of short radio waves during changing weather conditions.

The second set of plots (Figs. 23-36) shows the height distribution of the ratios C_e^2/C_T^2, C_{eT}^2/C_T^2 and C_N^2/C_T^2 for a variety of air masses and locations. These quantities are calculated from equations (8), (9), and (10). The assumption on which these plots are based is relatively defensible, requiring only that the quantities e_p, θ, and ϕ be mixed by turbulence in the same way; it is generally assumed that the eddy coefficients of the various conserved quantities are virtually the same. Because we deal with ratios, we need assume nothing about the intensity of mechanical turbulence.

The incentive for these plots is the belief that more measurements exist for C_T^2 (or the C_n^2 for optical refractive index) than exist for the C_N^2 of radio refractive index. Therefore, these plots permit one to make use of measurements made for optical systems to infer the scattering and scintillation characteristics of the atmosphere for radio waves.

Figs. 37, 38, and 39 show the distribution of C_n^2 with height in various air masses, where C_n^2 is the structure constant for optical wavelengths. To make these calculations from mean temperature profile information, it was necessary to assume that the temperature variance caused by vertical mixing was proportional to the square of the height gradient of potential temperature. The validity of this assumption requires that the

mixing length, L, be statistically independent of air mass type and height within the air mass. After plotting profiles of $(\Delta\theta/\Delta z)^2$ for the various air masses, the plots were "calibrated" in terms of C_n^2 by assuming the Hufnagel model to represent a median profile for the various air masses. Hufnagel's model is shown superimposed on Fig. 38. It is evident that the scatter of the air mass profiles about the Hufnagel profile is very large. However, measured profiles deduced from optical scintillation of stars show great scatter also, as seen in Fig. 40, from Ochs *et al.* (1976). In the calculated profiles C_n^2 occasionally drops to very low values. This occurs in height regions where the temperature gradient is very nearly the adiabatic lapse rate. There is some evidence of such deep troughs in the data of Ochs *et al.* even though the measurement technique had poor height resolution and must have smoothed the true profiles appreciably. These data were acquired in just one location (Boulder, Colorado) on only a few days.

Finally, having calculated the profiles of the optical structure constant, we can calculate the profiles of radio refractive index structure function with no additional assumptions. These profiles are shown in Figs. 41, 42, and 43 and are labeled C_N^2 to distinguish them from the optical refractive index structure constant labeled C_n^2; however, C_N^2 has not had the factor 10^{-6} removed from the refractive index as has N in Eq. (1b) and so differs from the structure constant of N by the factor 10^{-12}. There are several points worth noting:

1) The value of radio C_N^2 is not always larger than the optical C_n^2. Note, for example, the topmost value in winter cP air at Oklahoma City. This occurs when temperature and moisture fluctuations are positively correlated. Then the last term in Eq. (8) can potentially subtract more

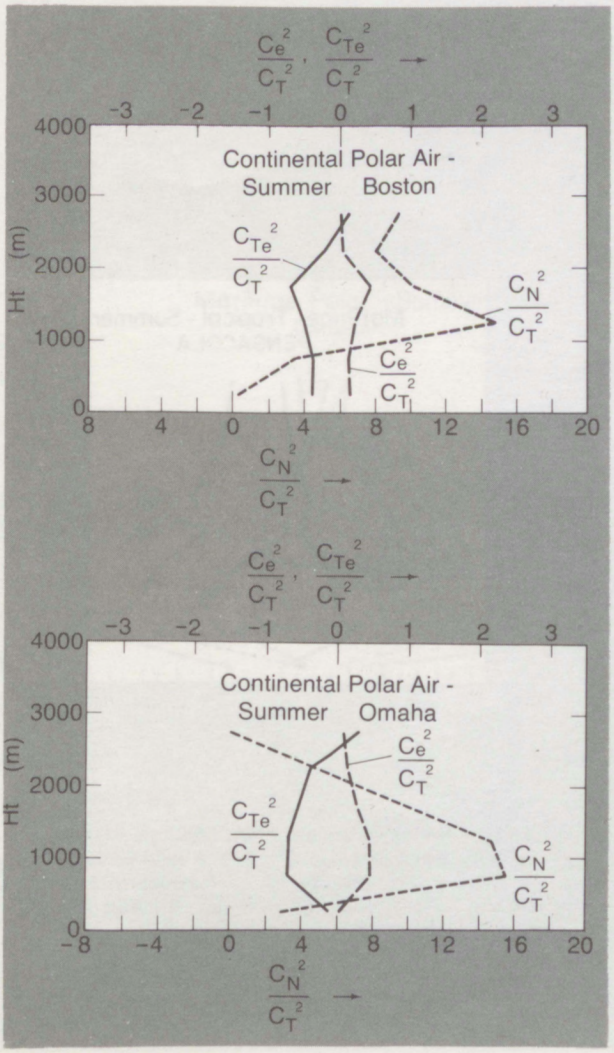

Figure 23. Ratios of the structure constant of refractive index and humidity to the structure constant of temperature for various North American air masses at the season and location indicated.

Figure 24. Ratios of the structure constant of refractive index and humidity to the structure constant of temperature for various North American air masses at the season and location indicated.

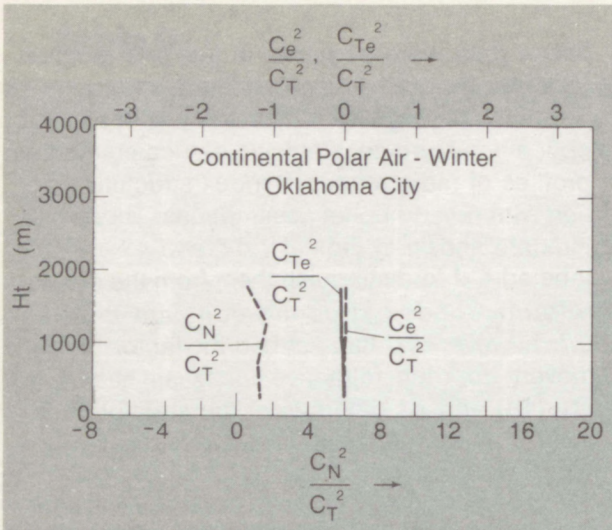

Figure 25. Ratios of the structure constant of refractive index and humidity to the structure constant of temperature for various North American air masses at the season and location indicated.

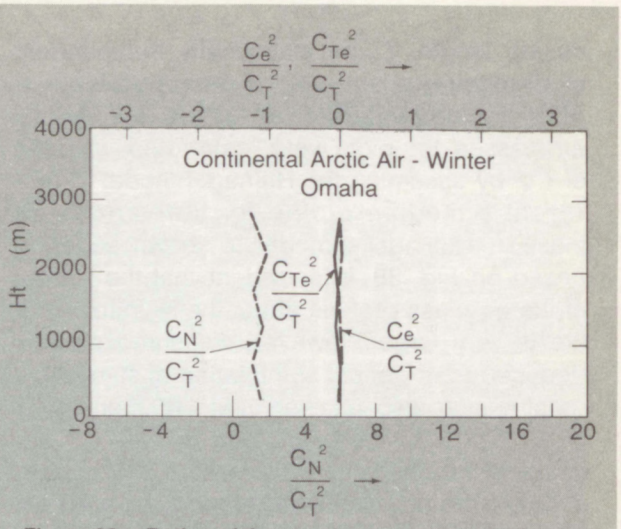

Figure 26. Ratios of the structure constant of refractive index and humidity to the structure constant of temperature for various North American air masses at the season and location indicated.

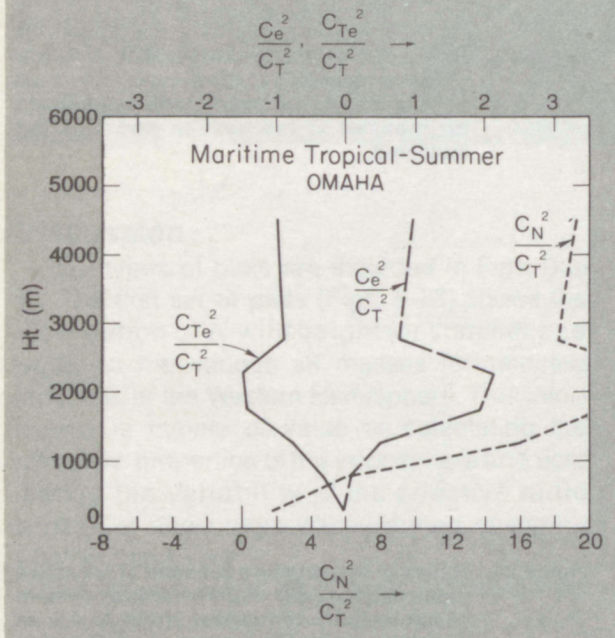

Figure 27. Ratios of the structure constant of refractive index and humidity to the structure constant of temperature for various North American air masses at the season and location indicated.

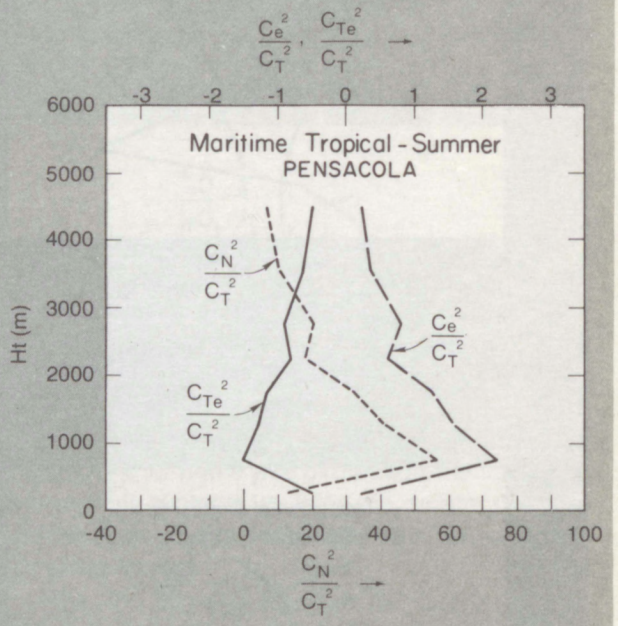

Figure 28. Ratios of the structure constant of refractive index and humidity to the structure constant of temperature for various North American air masses at the season and location indicated.

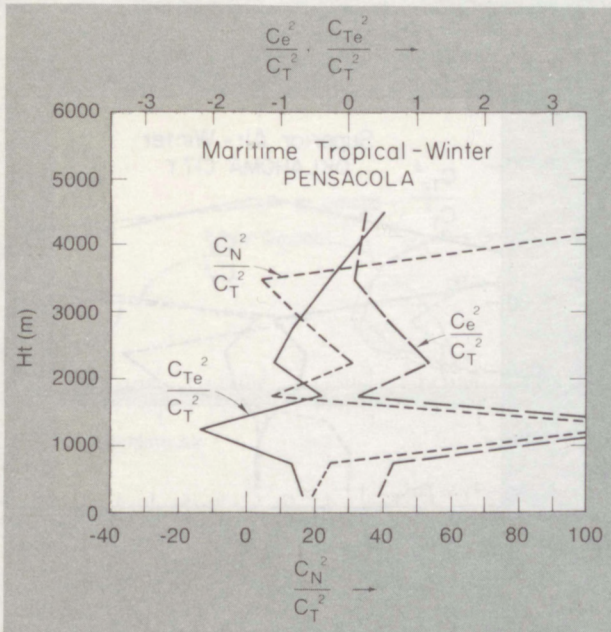

Figure 29. Ratios of the structure constant of refractive index and humidity to the structure constant of temperature for various North American air masses at the season and location indicated.

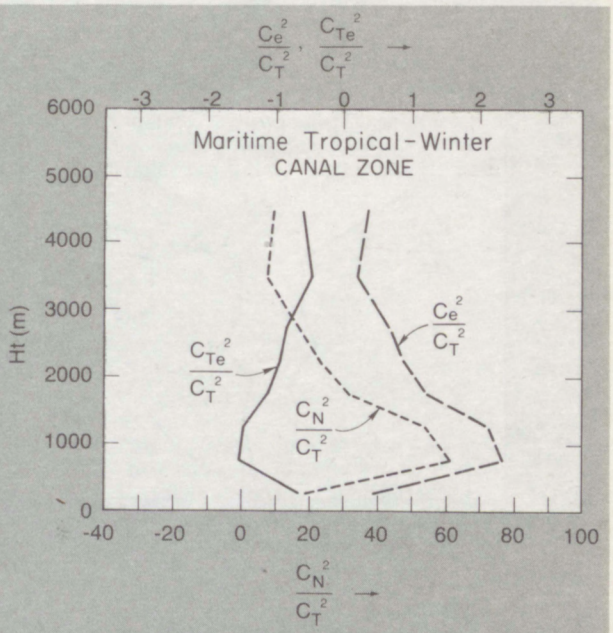

Figure 30. Ratios of the structure constant of refractive index and humidity to the structure constant of temperature for various North American air masses at the season and location indicated.

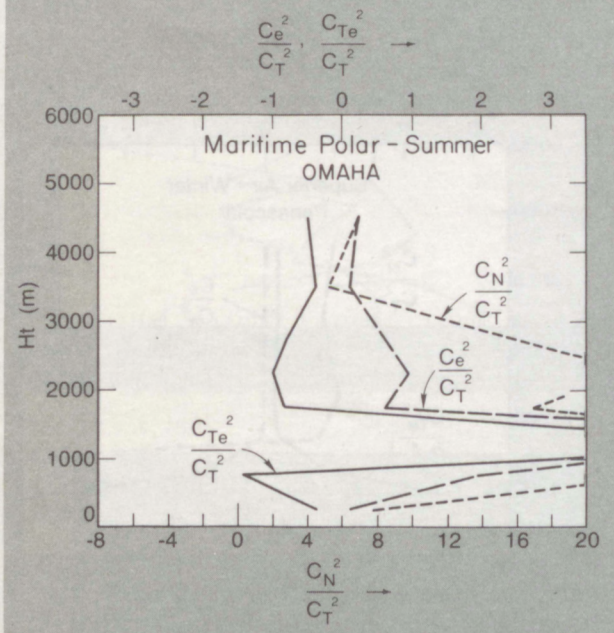

Figure 31. Ratios of the structure constant of refractive index and humidity to the structure constant of temperature for various North American air masses at the season and location indicated.

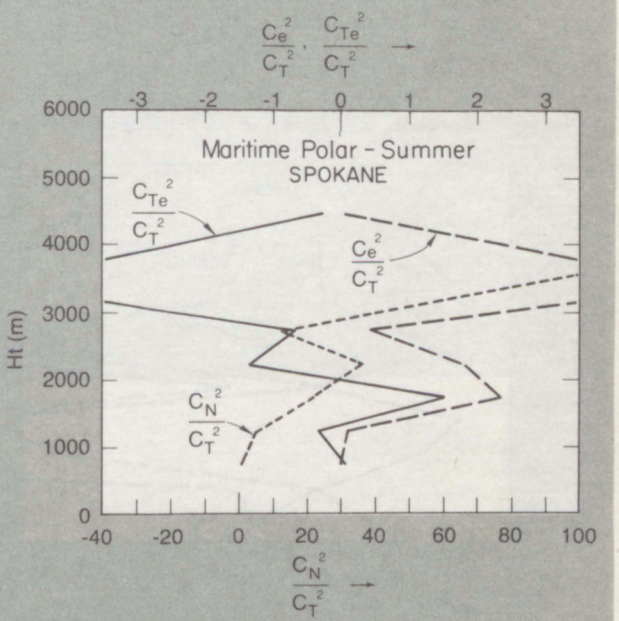

Figure 32. Ratios of the structure constant of refractive index and humidity to the structure constant of temperature for various North American air masses at the season and location indicated.

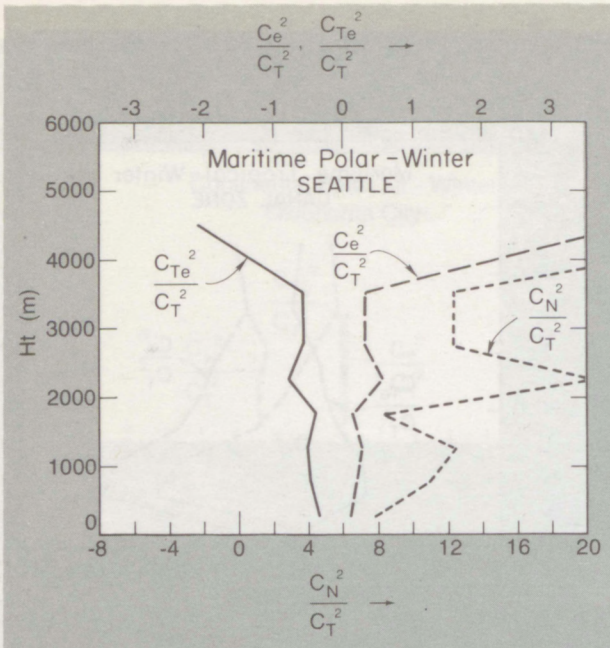

Figure 33. Ratios of the structure constant of refractive index and humidity to the structure constant of temperature for various North American air masses at the season and location indicated.

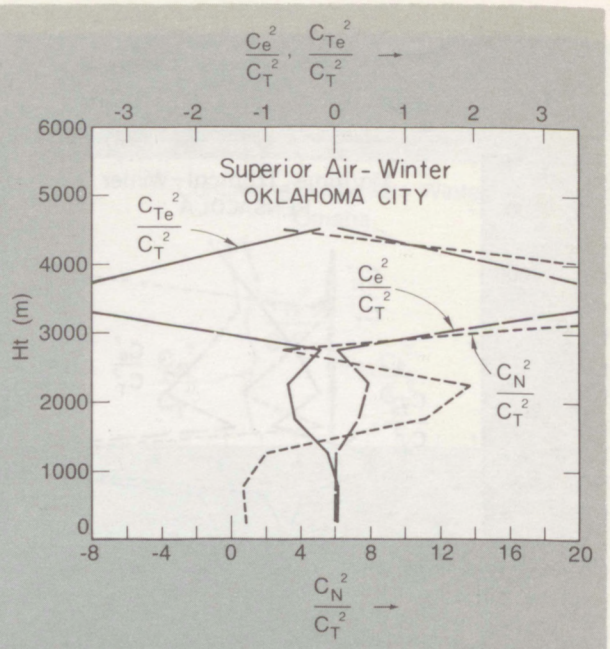

Figure 34. Ratios of the structure constant of refractive index and humidity to the structure constant of temperature for various North American air masses at the season and location indicated.

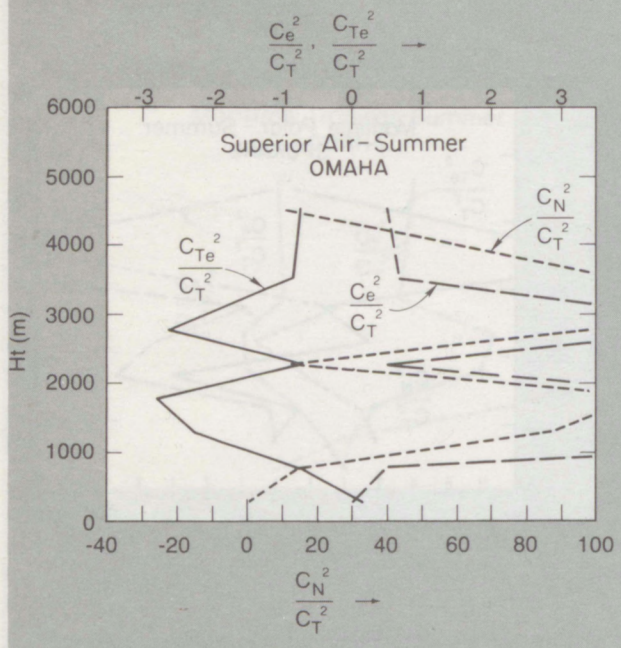

Figure 35. Ratios of the structure constant of refractive index and humidity to the structure constant of temperature for various North American air masses at the season and location indicated.

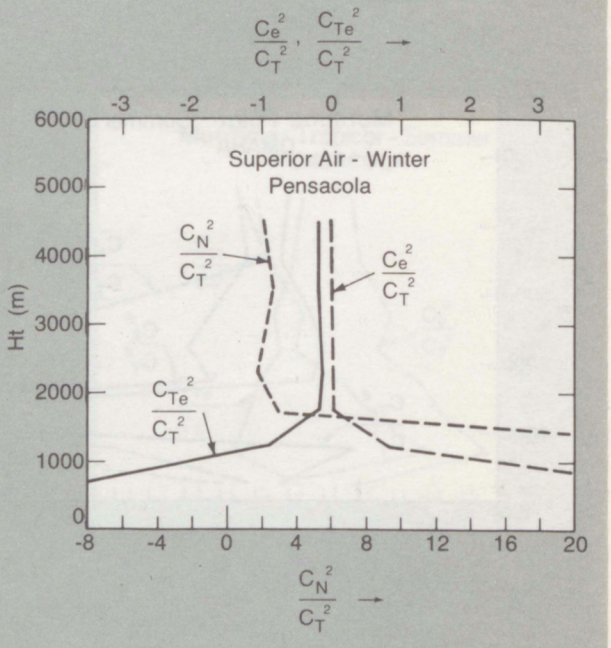

Figure 36. Ratios of the structure constant of refractive index and humidity to the structure constant of temperature for various North American air masses at the season and location indicated.

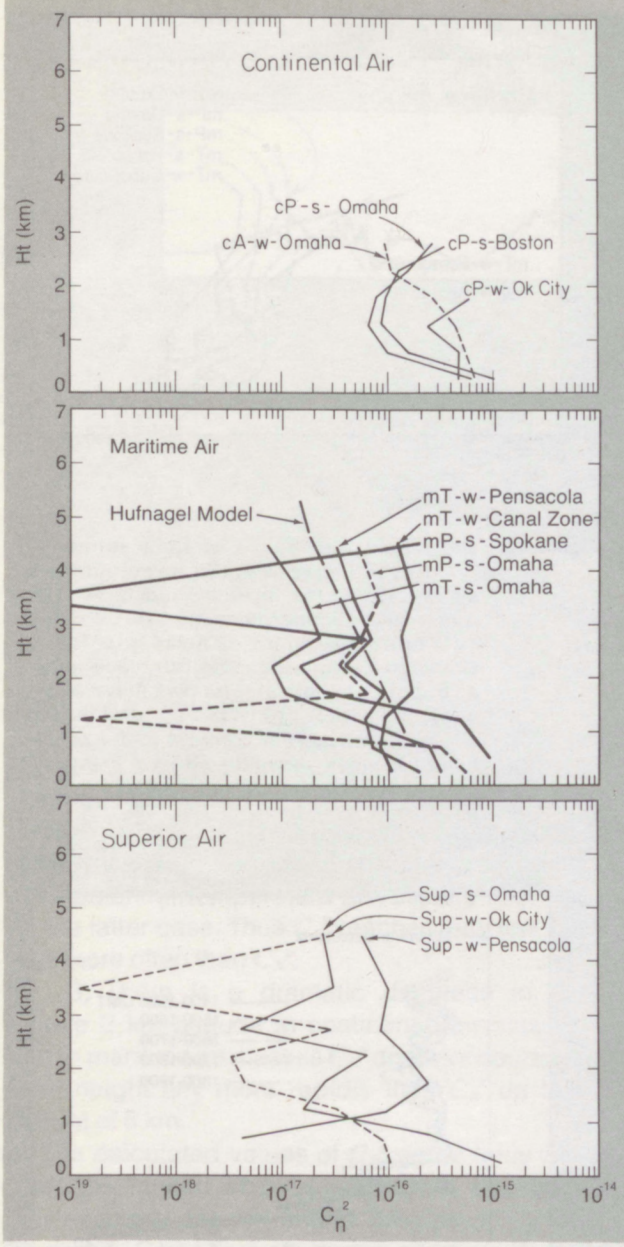

Figure 37. Distribution of optical refractive index structure constant in continental air masses at the locations shown. The winter and summer seasons are indicated by the small s and w following the air mass type. C_n^2 is in $m^{-2/3}$.

Figure 38. Distribution of optical refractive index structure constant in maritime air masses at the locations shown. The winter and summer seasons are indicated by the small s and w following the air mass type. C_n^2 is in $m^{-2/3}$.

Figure 39. Distribution of optical refractive index structure constant in superior air masses at the locations shown. The winter and summer seasons are indicated by the small s and w following the air mass type. C_n^2 is in $m^{-2/3}$.

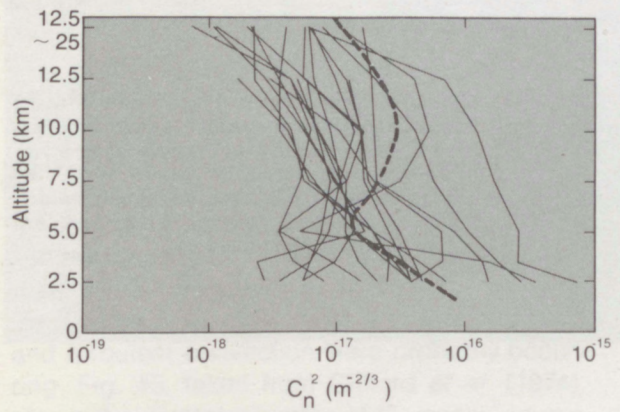

Figure 40. Measured distribution of optical refractive index structure constant compared with Hufnagel model indicated by dashed curve. (From Ochs *et al.*, 1976).

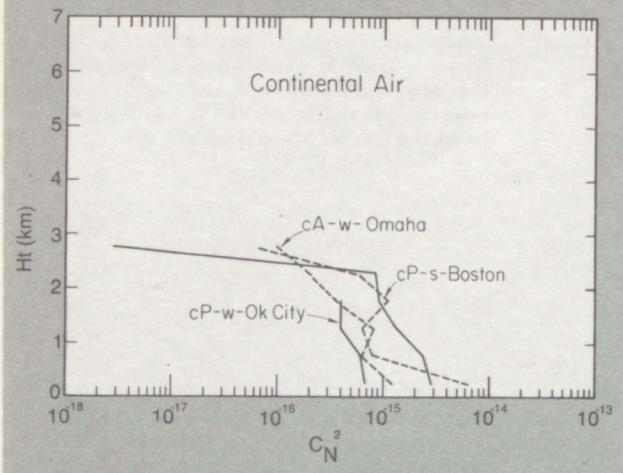

Figure 41. The height distribution of radio refractive index structure constant in some continental air masses at the location indicated. The winter and summer seasons are indicated by w or s following the air mass type. The N subscript designates radio refractive index as opposed to optical refractive index. However, the factor $(10^{-6})^2$ is included in this structure constant in contrast to the definition of N given above Eq. (1b). C_N^2 is in $m^{-2/3}$.

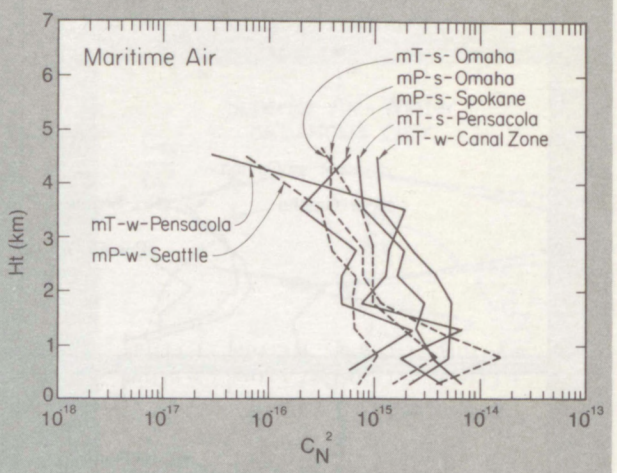

Figure 42. The height distribution of radio refractive index structure constant in some maritime air masses at the locations indicated. The winter and summer seasons are indicated by w or s following the air mass type. The N subscript designates radio refractive index as opposed to optical refractive index. However, the factor $(10^{-6})^2$ is included in this structure constant in contrast to the definition of N given above Eq. (1b). C_N^2 is in $m^{-2/3}$.

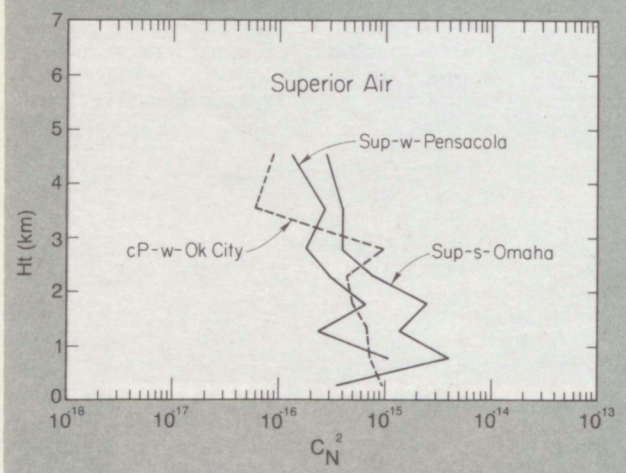

Figure 43. The height distribution of radio refractive index structure constant in some superior air masses at the locations indicated. The winter and summer seasons are indicated by w and s following the air mass type. The N subscript designates radio refractive index as opposed to optical refractive index. However, the factor 10^{-12} is included in this structure constant in contrast to the definition of N given above Eq. (1b). C_N^2 is in $m^{-2/3}$.

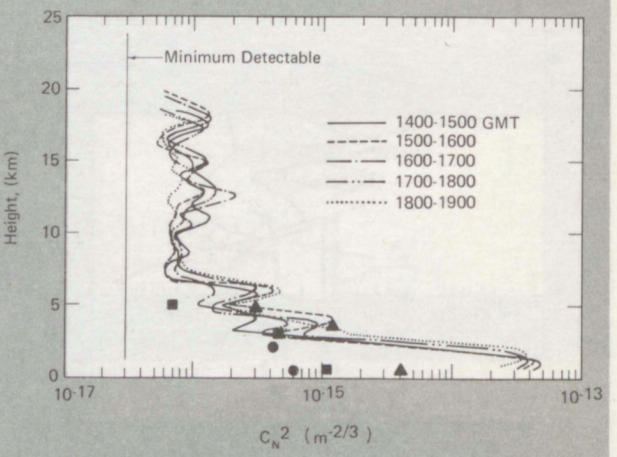

Figure 44. Measured height distribution of radio refractive index structure constant recorded with the Millstone Hill radar at the times indicated in December, reported by Crane, 1970. The circles, squares, and triangles are calculated values for winter cP, winter mP, and winter mT air masses, respectively.

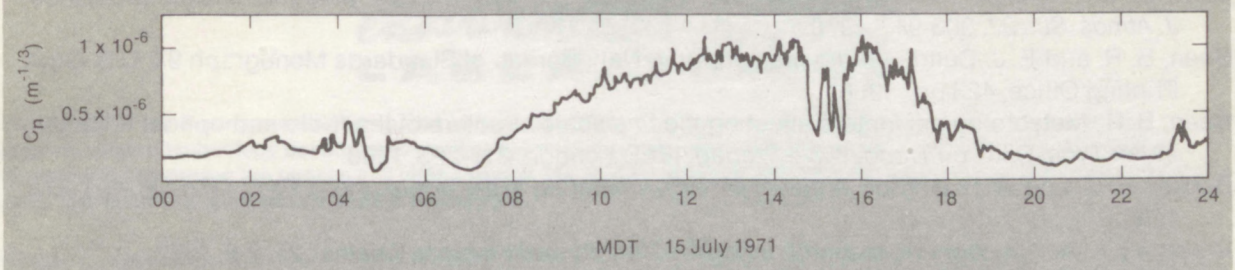

Figure 45. Diurnal distribution of C_n measured at a height of 2 m above the ground. (From Clifford *et al.*, 1974).

from C_N^2 than is contributed by the moisture (middle term). This occurs when moisture increases with height, because potential temperature must always increase with height (except in rare superadiabatic layers) in order that the atmosphere be statically stable.

2) The scatter of C_N^2 is less than that of C_n^2. This is because the temperature lapse rate approaches the adiabatic more often than the gradient of potential refractive index approaches zero since nearly zero gradients of both humidity and potential temperature are usually required in the latter case. Thus C_n^2 reaches very low values more often than C_N^2.

3) There is a dramatic decrease in C_N^2 above 2 km altitude in continental air masses, but in maritime air masses C_N^2 does not decrease with height any more rapidly than C_n^2 up to a height of 5 km.

The calculated values of C_N^2 agree fairly well with the limited observational data available. For example, Fig. 44 shows profiles of C_N^2 reported by Crane (private communication). These data were collected by the large, powerful Millstone Hill L-Band radar in December 1967. At that time of year one of three air masses might well have been in the area. Consequently, points representative of winter cP (circles), winter mP (squares), and winter mT (triangles) air masses were superimposed on Crane's data. The agreement is generally satisfactory except for the surface values. This discrepancy probably represents a diurnal effect, as Crane's observations were made near mid-day when surface heating and turbulent convection were probably occurring. Fig. 45, taken from Clifford *et al.* (1974), shows the diurnal variation of C_n measured at a height of 2 m. Apparently more than an order-of-magnitude enhancement in C_n^2 is to be expected around mid-day. Such an enhancement would bring our calculated values into good agreement with Crane's observations. ■

REFERENCES

Atlas, D., J. I. Metcalf, J. H. Richter, and E. E. Gossard, The birth of "CAT" and microscale turbulence, *J. Atmos. Sci. 27,* 903-913, 1970.

Bean, B. R. and E. J. Dutton, *Radio Meteorology,* Natl. Bureau of Standards Monograph 92, U.S. Govt. Printing Office, 423 pp., 1966.

Bean, B. R., Meteorological factors affecting the fine scale structure of the radio and optical refractive index, *Proc. Conf. on Tropo. Wave Propag.* IEEE, London, 217-223, 1968.

Booker, H. G. and W. E. Gordon, A theory of radio scattering in the troposphere, *Proc. I.R.E. 38,* 401-412, 1950.

Browning, K. A., Atmospheric research using the Defford radar facility, *Weather 27,* 2-8, 1972.

Chadwick, R. B., K. P. Moran, R. G. Strauch, G. E. Morrison, and W. C. Campbell, Microwave radar wind measurements in the clear air, (submitted for publication) 1976.

Chromov, S. P., *An Introduction to Synoptic Analysis,* 2nd Edition, Hydrometeorological Office, Moscow, 1937.

Clifford, S. F., G. R. Ochs, and R. S. Lawrence, Saturation of optical scintillation by strong turbulence, *J. Optical Soc. of Amer. 64,* 148-154, 1974.

Crane, R. K., Measurement of clear air turbulence in the lower stratosphere using the Millstone Hill L-Band Radar, *Preprints, 14th Weather Radar Conf.,* Amer. Meteorol. Soc., Boston, Mass., 101-106, 1970.

Gossard, E. E., Power spectra of temperature, humidity and refractive index from aircraft and tethered balloon measurements, *I.R.E. Trans. on Antennas and Propagation AP-8,* 186-201, 1960.

Gossard, E. E., J. H. Richter, and D. Atlas, Internal waves in the atmosphere from high-resolution radar measurements, *J. Geophys. Res. 75,* 3523-3536, 1970.

Hardy, K. A., Studies of the clear atmosphere using high power radar, Ch 14, *Remote Sensing of the Troposphere* (V. E. Derr, Editor), U.S. Govt. Printing Office, Washington, D.C., 1972.

Hufnagel, R. E., Variations of Atmospheric Turbulence, Proceedings Opt. Soc. Am. Topical Meeting on Optical Propagation through Turbulence, July 1974.

Kerr, D. E. (Editor), *Propagation of Short Radio Waves,* Dover, New York, 706 pp., 1951.

Ochs, G. R., Ting-i Wang, R. S. Lawrence, and S. F. Clifford, Refractive turbulence profiles measured by spatial filtering of scintillations, (submitted for publication) 1976.

Ottersten, H., Atmospheric structure and radar backscattering in clear air, *Radio Sci. 4,* 1179-1193, 1969.

Plank, V. G., Refractive properties of air masses, U.S. Navy Electronics Laboratory *Report No. 243,* 28 pp., 1952.

Richter, J. H., High resolution tropospheric radar sounder, *Radio Sci. 4,* 1261, 1969.

Showalter, A. K., Further studies of American air mass properties, *Mon. Wea.* Rev. 67, 204-218, 1939.

Strauch, R. G., W. C. Campbell, R. B. Chadwick, and K. P. Moran, Microwave FM-CW Doppler radar for boundary layer probing, *Geophys. Res. Letters 3,* 193-196, 1976.

Environmental Research LABORATORIES

The mission of the Environmental Research Laboratories (ERL) is to conduct an integrated program of fundamental research, related technology development, and services to improve understanding and prediction of the geophysical environment comprising the oceans and inland waters, the lower and upper atmosphere, the space environment, and the Earth. The following participate in the ERL missions:

MESA *Marine EcoSystems Analysis Program.* Plans, directs, and coordinates the regional projects of NOAA and other federal agencies to assess the effect of ocean dumping, municipal and industrial waste discharge, deep ocean mining, and similar activities on marine ecosystems.

OCSEA *Outer Continental Shelf Environmental Assessment Program.* Plans, directs, and coordinates research of federal, state, and private institutions to assess the primary environmental impact of developing petroleum and other energy resources along the outer continental shelf of the United States.

WM *Weather Modification Program Office.* Plans, directs, and coordinates research within ERL relating to precipitation enhancement and mitigation of severe storms. Its National Hurricane and Experimental Meteorology Laboratory (NHEML) studies hurricane and tropical cumulus systems to experiment with methods for their beneficial modification and to develop techniques for better forecasting of tropical weather. The Research Facilities Center (RFC) maintains and operates aircraft and aircraft instrumentation for research programs of ERL and other government agencies.

AOML *Atlantic Oceanographic and Meteorological Laboratories.* Studies the physical, chemical, and geological characteristics and processes of the ocean waters, the sea floor, and the atmosphere above the ocean.

PMEL *Pacific Marine Environmental Laboratory.* Monitors and predicts the physical and biological effects of man's activities on Pacific Coast estuarine, coastal, deep-ocean, and near-shore marine environments.

GLERL *Great Lakes Environmental Research Laboratory.* Studies hydrology, waves, currents, lake levels, biological and chemical processes, and lake-air interaction in the Great Lakes and their watersheds; forecasts lake ice conditions.

GFDL *Geophysical Fluid Dynamics Laboratory.* Studies the dynamics of geophysical fluid systems (the atmosphere, the hydrosphere, and the cryosphere) through theoretical analysis and numerical simulation using powerful, high-speed digital computers.

APCL *Atmospheric Physics and Chemistry Laboratory.* Studies cloud and precipitation physics, chemical and particulate composition of the atmosphere, atmospheric electricity, and atmospheric heat transfer, with focus on developing methods of beneficial weather modification.

NSSL *National Severe Storms Laboratory.* Studies severe-storm circulation and dynamics, and develops techniques to detect and predict tornadoes, thunderstorms, and squall lines.

WPL *Wave Propagation Laboratory.* Studies the propagation of sound waves and electromagnetic waves at millimeter, infrared, and optical frequencies to develop new methods for remote measuring of the geophysical environment.

ARL *Air Resources Laboratories.* Studies the diffusion, transport, and dissipation of atmospheric pollutants; develops methods of predicting and controlling atmospheric pollution; monitors the global physical environment to detect climatic change.

AL *Aeronomy Laboratory.* Studies the physical and chemical processes of the stratosphere, ionosphere, and exosphere of the Earth and other planets, and their effect on high-altitude meteorological phenomena.

SEL *Space Environment Laboratory.* Studies solar-terrestrial physics (interplanetary, magnetospheric, and ionospheric); develops techniques for forecasting solar disturbances; provides real-time monitoring and forecasting of the space environment.

U.S. DEPARTMENT OF COMMERCE
National Oceanic and Atmospheric Administration
BOULDER, COLORADO 80302